

RESEARCH ARTICLE

A Complete Affordable Control System for Remote Astronomical Observing Accompanied by an Intelligent Controller

MOHAMED ISMAIL¹, S. H. ELBANNA², MAHMOUD A. EL-DABAH²,
AND FARAG ELNAGAHY¹

¹Astronomy Department, National Research Institute of Astronomy and Geophysics (NRIAG), Cairo 11421, Egypt

²Electrical Engineering Department, Faculty of Engineering, Al-Azhar University, Cairo 11651, Egypt

Corresponding author: Mohamed Ismail (eng.m_email@yahoo.com)

This work was supported in part by the National Research Institute of Astronomy and Geophysics (NRIAG), and in part by the Kottamia Center of Scientific Excellence for Astronomy and Space Science (KCSCE) under Grant STDF 5217.

ABSTRACT This paper comprises two studies; the first one provides an advanced and low-cost implementation for a remote astronomical platform applicable to small and medium-sized telescopes. It has been carried out for the 14-inch observatory, which includes a Celestron German Equatorial (CGE) telescope at the Kottamia astronomical observatory (KAO) in Egypt. This integrated control system is based on embedded systems, internet of things (IoT) technology, row packets communication procedure, and the Transmission Control Protocol (TCP) based on the Internet Protocol (IP). Using this platform, remote astronomers could control the whole system, observe, receive images and view them efficiently and safely without any human physical intervention. The proposed design has been achieved without dependence on commercial control kits or software. Indeed, many previous studies have focused on this field; however, their area of interest was limited or non-affordable. The excellence in this practical research is revealed and compared with others in terms of cost, inclusiveness, and communication speed. The other contribution of this research is to enhance the performance of the telescope pointing and tracking to be adapted with remote action. It has been achieved based on the mathematical model of the telescope where two fractional controllers have been applied, tilt integral-derivative (TID) and integral derivative-tilted (ID-T) controllers. After that, they have been optimized using a recent optimization algorithm called the peafowl optimization algorithm (POA) and compared with one of the well-known algorithms, particle swarm optimization (PSO). Simulation results under the MATLAB/SIMULINK environment reveal that modified ID-T-based POA has minimized the pointing error sharply. Moreover, compared with previous studies, it has significantly improved the telescope system characteristics represented in overshoot, settling, and rising periods.

INDEX TERMS Remote telescope, integral derivative-tilted controller, peafowl optimization algorithm.

I. INTRODUCTION

Astronomers and astrophysicists from ancient to now are interested in sky objects observation, such as stars, planets, and galaxies translating observed images into discoveries [1] and data that analyze the universe's construction and our location inside it [2]. The astronomical observation is performed inside an observatory that comprises a

telescope, a dome, an image detector, and a weather station [3]. The optical telescopes gather emitted light from visible sky objects then concentrate it using mirrors [4]. Thus, optical observatories are consistently located at distant sites to offer better seeing, less atmospheric water vapor, and reduced light pollution [5]. Therefore, the attitude of developing telescopes to run remotely has grown exponentially to enable astronomers to perform observation from anywhere, avoiding traveling efforts toward the telescope's physical site.

The associate editor coordinating the review of this manuscript and approving it for publication was R. K. Tripathy¹.

Remote observation embeds the aspects of traditional observation such as checking the weather, opening dome enclosure, pointing the telescope, setting exposure time, and storing data; however, it is performed over the internet with the priority of protecting the telescope equipment [6]. Furthermore, it reduces the downtime of the observatory, minimizes the telescope setting up stress [7], decreases the operation cost, and the number of personnel required [8]. Moreover, It plays a more critical role in international projects in astronomical scientific research [9], and it is considered an easy tool for astronomy education at different levels [10].

Regarding the telescope performance, pointing and tracking accuracy is crucial in observing desired targets in the sky [11]. Moreover, excellent performance is essential to take advantage of remote telescope [12]. This could be achieved using intelligent controllers with advanced optimization techniques. Thus, fractional-order (FO) controllers like tilt integral-derivative (TID) and integral derivative-tilted (ID-T) will be utilized upon the telescope model using the MATLAB environment to minimize the error among desired and reference signals. Subsequently, optimization techniques based on artificial intelligence; peafowl optimization algorithm (POA) and particle swarm optimization (PSO), will be the tool for acquiring optimal values of the controller's gains.

A. LITERATURE REVIEW

Over recent years, remote control technology and sensors have continually evolved and advanced, giving the facility for remote observing development [13]. Because of the design of small and medium-sized observatories not supporting remote operation [14], several attempts have been implemented to upgrade them to run remotely at low cost. For instant, Iowa robotic observatory is considered the first operation of remote observation in the 1990s [15]. In Spain, the 0.25-meter telescope has been developed to observe remotely in real-time mode [16] and the Vixen equatorial telescope in Japan has been modified to be operated via the internet [9]. Moreover, the Koreans have converted their telescope into robotic using an embedded controller [17]. Required developments have been carried out for the MEADE-LX850 telescope to run remotely [18].

In deed, the earlier developers have utilized commercial software in remote operation, gathering weather data, and setting up the telescope. In addition, they have not achieved a proper alignment which is essential at startup to gain total control of the telescope, as well as the observatory does not make a decision automatically whether or not to open the dome based on the measurements, which is considered a great risk. Another theoretical analysis has produced in [19] and has focused on dome automation and protection from bad weather conditions; although this study provided a low-cost platform compared to commercial kits, it has not been implemented practically.

The CGE telescope comprises two direct currents (DC) motor drivers that are responsible for pointing it in right ascension (RA) from east to west and declination (DEC)

from north to south. The mathematical model of the telescope is based on a set of dynamic equations with nonlinear coupled differential equations that contain different terms for moments of inertia, a centrifugal and Coriolis, and a frictional term. It also includes a gravity term; however, it tends to zero in case of accurate telescope balance [20].

Studies have been interested in how to force the telescope to accelerate its motors at a suitable velocity for reaching the selected target in the desired position by controlling the telescope's joint torque. Thus, several controllers have been applied to keep the telescope pointing in reference trajectory with minimum error using different optimization techniques based on artificial intelligence. Based on previous research, the main conclusion is that the fuzzy logic control (FLC) strategies have provided moderate performance. However, FLC has flaws in terms of the rise time (R_s) and the settling time (T_s), which are not accepted in the case of robotic operation.

As shown in Table 1, FLC has been applied and optimized by a genetic algorithm (GA); even though the R_s was suitable, it produced an unacceptable overshoot (O_{sh}) [20]. The response with O_{sh} is an impermissible issue due to the use of a fixed charge-coupled device camera (CCD) on the telescope while tracking a sky object [21]. Moreover, although FLC that PSO drives have provided better performance according to previous techniques followed by proportional-integral-derivative (PID) controller tuned from FLC, they are not sufficient as the R_s was inappropriate in case of remote operation [22]. Furthermore, in the face of system uncertainties, conventional proportional-derivative (PD) and PID controllers have some difficulty as their defects of high O_{sh} and R_s are inappropriate.

TABLE 1. Characteristics survey of past research.

Control Technique	R_s (s)	T_s (s)	O_{sh} (%)
	RA - DEC	RA - DEC	RA - DEC
PD-GA	0.392 - 0.413	0.331 - 0.485	3.50 - 3.13
PID-PSO	0.062 - 0.061	0.400 - 0.350	22.2 - 20.0
PID-FLC	0.380 - 0.380	0.740 - 0.740	0 - 0
FLC- GA	0.200 - 0.304	0.331 - 0.485	0.5 - 0.45
FLC- PSO	0.335 - 0.330	0.750 - 0.600	0 - 0

B. CHALLENGES

Since the design of small and medium-sized observatories does not support remote operation [14], the modification requires extra hardware and software to overcome the absence of the human attendance [23]. The dome is represented the main obstacle toward remote operation as a reason for its manual operation in rotation and shutters handling [24]. In addition, the telescope itself always requires a set up before any observation using its hand control (HC), and the focus which has a great impact in image quality [25] is adjusted under watch without any physical limitations. Beginning with the hardware, it should be a robust control system, including a suitable controller, various sensors, and a

monitoring system. Moreover, the software interface should provide rapid response, automatic decision making, and several modes of operation. Finally, extra sensors, encoders, and devices like a weather station, monitoring system, and remote power unit should be installed in the observatory. Concerning the software interface, small and medium-sized telescopes depend on commercial products protected by a trademark; as a result, their accessories and programs are only compatible with Windows, which is not an open-source operating system [18]. Besides, the wireless operation often utilizes Team Viewer or other visual network computers (VNC) programs that require a highly stable network bandwidth unavailable in high-altitude observatories. In addition, it has a critical defect in data transfer delay as it transfers all events from a remote computer to a local one. Secure Shell (SSH) software is widely used in remote operation over Linux operating systems; nevertheless, it has a complexity in the command line, which user is often unfamiliar with it [26]. These factors complicate designing one graphical user interface, which makes the interface robust and communicated. The solution to overcome these restrictions is to write a complete code that manages the telescope and instruments.

Following modification of the telescope efficiency during pointing, the major challenge is selecting an efficient controller and extracting optimal gains using advanced optimization techniques. As mentioned before, astronomical observation requires precision parameters during observing via minimizing the error between desired and set positions of the sky coordinates. Therefore, the utilized controller should include superior characteristics in terms of its structure and tuning in order to achieve a minimum error besides eliminating O_{sh} with less R_s and T_s at the same time.

C. MOTIVATION

A preliminary study concerning transferring traditional telescopes to run remotely efficiently with affordable cost has flaws in terms of comprehensiveness and expense. Moreover, it is noteworthy that developers mostly interested in modifying just one item of the observatory, such as the telescopes, the dome, or the wireless communication tool. Furthermore, they frequently rely on costly commercial automation kits and programs. These defects provided a motivation to design and implement an observatory serviced remote facility beside keeping the cost affordable. It is an obvious fact that designing a remote control system for astronomical observation without the use of commercial control systems and software eliminates expensive budgets involved with the possibility for modification.

It has been noted that substantial past studies on enhancing the telescope performance in pointing had yielded limited benefits. FLC and conventional controllers, which have been optimized using different artificial intelligence techniques, have produced either overshoot or long rise time. These two factors are impermissible in the case of remote observation that requires a telescope with high-performance [6]. Moreover, these flaws prevent the anticipated advantage of remote

telescope from being realized, so it has been decided to use a sophisticated controller to achieve the most satisfactory outcomes. The authors intend to modify the CGE controller in the future; therefore, the theoretical study is necessary to decide which controller will provide the best response.

D. CONTRIBUTION AND PAPER ORGANIZATION

This practical study includes creating a complete control system for the telescope, the dome, the camera, the focus system, and associated devices. It covers all aspects of observation with self-protection against natural hazards, faults, and interruptions. Furthermore, no commercial kits or software have been used, and as a result, the cost was overly small compared to commercial systems and previous research. Moreover, remote access is designed based on the Transmission Control Protocol and the Internet Protocol (TCP-IP) client-server socket, which perfectly offers numerous utilities that enhance the performance and security of accessing and transferring data between the server and clients [27].

The another contribution in this paper is involved in applying the fractional TID and ID-T controllers. FO controllers such as TID and ID-T have proliferated due to their flexibility in designing and stability, particularly with dynamical systems [28]. They include extra tuning parameters compared with conventional PID controller, which reduces processing in optimum parameters demonstration [29]. FO controllers are distinguished with more expanded freedom in tuning for system stabilizing, so researchers have a great interest in such controllers [30]. Moreover, the TID family is potentially one of the best FO controllers as it has a robustness in estimating the parameters of a system with a closed-loop enhancing the system response [31]. As well as, gains tuning is performed using different optimization techniques such as POA and PSO. The POA technique replicates the peafowls swarm behavior in their foraging, chasing, and courtship, where a triple group of peafowls (i.e., peafowl cubs, peacocks, and peahens) emulate the behaviors of dynamic swarm and hierarchy in food searching. It is considered an efficient exploratory searching operator and adaptive searching as well [32]. Simulation results and comparison diagrams imply that the response characteristics of the pointing position have been enhanced by minimizing the times of overshoot, rising, and settling.

The outlines starts with the introduction and followed by the construction and operation of the 14-inch observatory. After that, the automation process is revealed separately for each device and remote operation preparation. The section after that summarizes the overall control system, while the graphical user interface section comes after. Subsequently, the CGE telescope model and proposed controller are presented. The next section is the results with discussion and finally, a conclusion is provided.

II. SPECIFICATION OF THE 14-INCH OBSERVATORY

This section provides a detailed description of the 14-inch observatory before any modification when

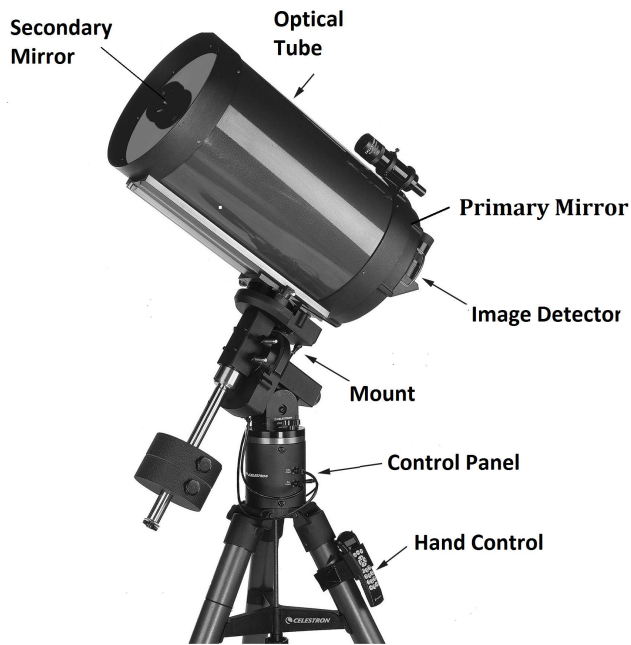


FIGURE 1. The 14-inch CGE telescope.

the observer was unable to perform the observation remotely.

A. THE 14-INCH CGE TELESCOPE

The 14-inch CGE telescope is located at the Kottamia observatory at a latitude of $29^{\circ} 55' 48''$ North and a longitude of $31^{\circ} 49' 30''$ East; height = 476 meters, about 70-kilo meters east of Cairo city [33]. Its optics is a Schmidt-Cassegrain designed with enhanced coatings for the primary mirror and the secondary to maximize the reflectivity. The telescope focal length is 3910 mm and focal ratio of F/11 with aluminum tube, while the mount is a computerized German equatorial type, as shown in Fig. 1 [34]. The driving system of the telescope depends on two DC motors working together to point and track sky objects based on integrated optical encoders with 0.11 arc second resolution [21]. It contains a control panel with three registered jacks (RJ) ports; RJ-45 for RA, DEC, and auto guider with two RJ-22 sockets for global positioning system (GPS) and HC. There are two built-in limit switches for the mount home position. The HC is a double-line, 16-character liquid crystal display (LCD); it is to control the mount and attached GPS manually. There is also a Recommended Standard-232 (RS-232) port located on the bottom of the HC for the computer communication [34]. The focus mechanism depends on adjusting the distance between the two mirrors by moving the primary mirror over a baffle tube. This motion is achieved via a bipolar stepper motor with a hand set (HS) to adjust the focus manually using two buttons in two directions. This HS is connected to the computer via the Universal Serial Bus (USB2) protocol to adjust focus computationally by commercial software named Micro Touch [35].



FIGURE 2. The 14-inch Ash dome.

B. ASTRONOMICAL DOME

The astronomical dome is the enclosure of the telescope and attached devices inside the observatory; it is necessary to protect them from the horrible weather conditions [36]. The 14-inch telescope dome is a hemisphere steel Ash-dome shown in Fig. 2 with approximately 5 meters in diameter and located upon a concrete wall. Dome rotation is driven via a three-phase, 1370 rpm, and 0.37 KW induction motor. This motor is fixed on the concrete wall and driven through a variable frequency drive to control the rotation speed. The mechanical motion is transferred from the motor to the dome through a circular iron gear fixed with the dome. The dome often includes an upper and a bottom shutters to form a dome slit providing a viewing aperture for the telescope during observation, even during windy conditions. The upper shutter is of the “up and over” and driven with a 200-watt DC motor. Meanwhile, the bottom takes some cranking to laterally raise and lower the shutter through a 600-watt single-phase induction motor. The observer uses a selector switch to rotate the dome left and right and push buttons to control the shutters [37].

C. IMAGING SYSTEM

The CCD camera is widely used in astronomy; it is an integrated circuit consisting of a certain number of coupled capacitors [18]. The utilized CCD camera is SBIG version STX-16803 with 16 megapixels and a resolution of 4096×4096 pixels. It has two chips for imaging and guiding to enable imaging and self-guiding simultaneously. Cooling techniques are based on intelligent fans and connect with a water cooling technique [38]. There is an SBIG FW7-STX filter wheel equipped with the camera via the inter-integrated circuit I^2C protocol. It comprises 7-position, 50-millimeter

square filters with an optical encoder for position centering. Digital interface is available within two different protocols, USB2 and Ethernet where imaging is performed under window operating system via a commercial software named MaxIm-DL.

III. AUTOMATION OF THE 14-INCH OBSERVATORY AND REMOTE OPERATION REHABILITATION

Traditional astronomical observation starts with a weather condition check by either eye or a weather station. If it is valid, the observer opens the shutters, switches the light off, and then points the telescope toward a specified target in the sky. After that, he rotates the dome to keep its slit in front of the telescope direction, sets an exposure time for the CCD camera, and adjusts the focus. The telescope will track the observed object, which leads to changing its position, so the dome slit has to follow the new position to achieve dome synchronization. The sequence starts at the end of the night with parking the telescope and the dome, closing the shutters, and switching off all devices. In order to work toward an efficient remote observation with a robotic facility is a challenge as various aspects should be considered for unattended approach [26]. Moreover, it is prohibitively expensive to retrofit older control systems of the observatories to be operated remotely without direct human control [7]. The remote control system which has to be designed to safely control the telescope, the dome, the CCD camera, and auxiliary instruments [12].

A. TELESCOPE CREATION

As mentioned before, the observer has a choice to point the telescope manually using the HC buttons or via computer software as well. However, he cannot adjust the telescope effectively unless the setting up process is executed manually via the HC. Setting up the telescope involves two main processes; home position and alignment. Equatorial telescopes should be aligned for accurate pointing and tracking [39]; otherwise, the coordinate values will not be meaningful [40]. Moreover, it conflicts with remote telescope operations. For instant, the 14-inch MEADE telescope could not receive commands properly except when the telescope is in correct alignment at startup, and it is not possible to be performed except via its HC directly using manual buttons [18]. The alignment step is achieved by pointing the telescope to two bright reference stars; however, the observed stars will be shifted from the center of the image frame. Therefore, the user has to center them manually and press the Align button on the HC. By using these steps, the telescope will calculate the pointing error and store it [41]. In order to overcome this problem, the key lies in the data transferred between the telescope mount and the HC; extracting these data packets will be the solution. In order to obtain these commands that responsible for setting up the telescope, reverse engineering has become the convenient solution for extracting the packets transferred among the HC and the telescope mount while setting up the telescope. It has been achieved by inserting a computer with

TABLE 2. Home position packets description.

Packet	Response
0x50 0x01 0x10 0x0b 0x00 0x00 0x00 0x00	#
0x50 0x01 0x11 0x0b 0x00 0x00 0x00 0x00	#
0x50 0x01 0x10 0x12 0x00 0x00 0x00 0x01	00 or ff
0x50 0x01 0x11 0x12 0x00 0x00 0x00 0x01	00 or ff

TABLE 3. Last alignment packets description.

Packet	Response
0x50 0x04 0x10 0x04 0x40 0x00 0x00 0x00	#
0x50 0x04 0x11 0x04 0x40 0x00 0x00 0x00	#
0x50 0x04 0x10 0x3a 0xc0 0x00 0x00 0x00	#
0x50 0x01 0x10 0x38 0x00 0x00 0x00 0x00	#
0x50 0x04 0x11 0x3a 0xc0 0x00 0x00 0x00	#
0x50 0x04 0x11 0x3a 0xc0 0x00 0x00 0x00	#
0x50 0x04 0x10 0x0a 0x00 0x00 0x00 0x00	#
0x50 0x04 0x11 0x06 0x00 0x00 0x00 0x00	#
0x50 0x03 0x10 0x06 0xff 0xff 0x00 0x00	#

a custom code between them for spying on serial packets for commands and responses. Table 2 reveals the home position acquired packets for commands and responses among HC and the mount. After analyzing them, it has appeared that packets 1 and 2 are sent to move the telescope in two directions; RA and DEC, then packets 3 and 4 are continually sent with a "00" response until the exchange to "ff." This response indicates that the telescope is at the home position parking. Command format is as following: 0×50 <message Length> <destination Id> <message Id> <data1> <data2> <data3> <response Bytes>, where <data1> are the message data bytes and If there is empty data byte it must be represented by zero, while <responseBytes> is the echo back's byte number [42]. For instant if the hexadecimal PC command is to get the HC version, the packet will be in this form; $(0 \times 50 0 \times 01 0 \times 11 0 \times fe 0 \times 00 0 \times 00 0 \times 00 0 \times 02)$ and the response from the HC will be $(0 \times 04 0 \times 03 0 \times 23)$ which is 04.03 in decimal.

On the other hand, Table 3 displays acquired packets for the alignment process. These packets set the telescope coordinates to the last alignment correction values. The CGE written software relies on a communication protocol regarding the HC that instructs how to send commands to the telescope and get a response; it does not include the setting up commands. Talking to the mount is based on RS-232 serial commands in row hexadecimal packets covering all HC operating aspects [40] and has been executed by connecting a serial cable between the HC and the computer. Furthermore, the user could send raw commands to the telescope through a custom graphical window. Eventually, the mentioned packets will enable the observer to point the telescope efficiently and read its position in a coordinate system based on motors positions named setting circles.

The CGE telescope mount receives and sends coordinates in two different coordinate systems; one of them is through

the equatorial system, i.e., RA, DEC, which is a widely-used method of specifying the positions of celestial objects [17] while the other is axis position coordinates represented in the setting circle. Because the astronomer often uses equatorial coordinates during observation, conversion from the equatorial coordinates into the axis position coordinates became necessary to enable the remote observer to point the telescope normally. Eqs. 1 and 2 convert the equatorial coordinates (α , δ) into horizontal coordinates (ϕ , ψ); the horizontal coordinate is a celestial coordinate system that uses the observer's local horizon as the fundamental plane. Then Eqs. 3 and 4 produce the setting circle positions (j , q) from the horizontal coordinates [43].

$$\phi = \tan^{-1}[\sin H / (\cos H \sin \Gamma - \tan \delta \cos \Gamma)], \quad (1)$$

$$\psi = \sin^{-1}[\sin \Gamma \sin \delta + \cos \Gamma \cos \delta \cos H], \quad (2)$$

$$j = \tan^{-1}[\sin \phi / (\cos \phi \sin \Gamma + \tan \psi \cos \Gamma)], \quad (3)$$

$$q = \sin^{-1}[\sin \Gamma \sin \psi - \cos \Gamma \cos \psi \cos \phi], \quad (4)$$

where α , δ , ϕ , and ψ are the RA, DEC, azimuth, and altitude, respectively, while Γ is the telescope latitude. H is the hour angle which is a time relation with the RA and calculated from Eqs. 5 and 6 using the local sidereal time (β), the current Julian day (JD), and the telescope longitude (L) [43].

$$H = \beta - \alpha. \quad (5)$$

$$\beta = [(JD - 2451545) / 36525] + L, \quad (6)$$

where the numbers; 2451545 and 36525 are the JD corresponding to the date of Jan 2000 and the number of days of a century respectively.

Now, the pointing challenge is achieved; however, the observer needs to get a mount position in equatorial form. Therefore, Eqs. 7 and 8 convert the axis position coordinates into the horizontal coordinates then the equatorial coordinates are calculated from the previous Eq. 3 and 4 to get (H , δ). After that, Eqs. 5 and 6 produce the RA (α) [43].

$$\phi = \tan^{-1}[\sin j / (\cos j \sin \Gamma - \tan q \cos \Gamma)]. \quad (7)$$

$$\psi = \sin^{-1}[\sin \Gamma \sin q + \cos \Gamma \cos q \cos j]. \quad (8)$$

The telescope is permanently located at its dome at the Kottamia observatory, meaning that the alignment process is performed once by an expert [7]. Meanwhile, during remote observation, the observer may recall the last alignment correction. However, excessive motion during pointing may produce tiny pointing errors from mechanical parts and coupling. Therefore, designing an advanced option for remote alignment and correction is essential. The pointing correction starts with pointing the telescope into two bright stars and then center them in the frame remotely. Equatorial coordinates, time of pointing, and the axis position coordinates will be stored after the star centering process is finished. The modified correction procedure will convert these axis position coordinates into the horizontal coordinates. By applying a set of transformation equations, the alignment correction is achieved, and the accuracy of pointing will be

enhanced sharply [44]. The Mentioned stored coordinates are performed in Eqs. 9 and 10 to calculate parameters $l2$, $m2$, $n3$, $L1$, $M1$, and $N1$, after that the same two equations will be applied for the second star to calculate $l2$, $m2$, $n2$, $L2$, $M2$, and $N2$. By making use of all calculated values, $l3$, $m3$, $n3$, $L3$, $M3$, and $N3$ will be the output from Eqs. 11 - 14 then T is estimated as in Eq. 15.

$$\begin{bmatrix} l1 \\ m1 \\ n1 \end{bmatrix} = \begin{bmatrix} \cos \psi 1 \cos \phi 1 \\ \cos \psi 1 \sin \phi 1 \\ \sin \psi 1 \end{bmatrix}. \quad (9)$$

$$\begin{bmatrix} L1 \\ M1 \\ N1 \end{bmatrix} = \begin{bmatrix} \cos \delta 1 \cos \alpha 1 - k(t1 - t0) \\ \cos \delta 1 \sin \alpha 1 - k(t1 - t0) \\ \sin \delta 1 \end{bmatrix}, \quad (10)$$

where $t1$ and $t0$ are the first stars of observing time and the initial time of starting observation for remote alignment, respectively; meanwhile, k is a constant with a value of 1.002738.

$$\begin{bmatrix} l3 \\ m3 \\ n3 \end{bmatrix} = \frac{1}{\sqrt{Z}} \begin{bmatrix} m1 n1 - n1 m2 \\ n1 l2 - l1 n2 \\ l1 m2 - m1 l2 \end{bmatrix}. \quad (11)$$

$$Z = (m1 n1 - n1 m2)^2 + (n1 l2 - l1 n2)^2 + (l1 m2 - m1 l2)^2. \quad (12)$$

$$\begin{bmatrix} L3 \\ M3 \\ N3 \end{bmatrix} = \frac{1}{\sqrt{Y}} \begin{bmatrix} M1 N1 - N1 M2 \\ N1 L2 - L1 N2 \\ L1 M2 - M1 L2 \end{bmatrix}. \quad (13)$$

$$Y = (M1 N1 - N1 M2)^2 + (N1 L2 - L1 N2)^2 + (L1 M2 - M1 L2)^2. \quad (14)$$

$$[T] = \begin{bmatrix} l1 & l2 & l3 \\ m1 & m2 & m3 \\ n1 & n2 & n3 \end{bmatrix} \begin{bmatrix} L1 & L2 & L3 \\ M1 & M2 & M3 \\ N1 & N2 & N3 \end{bmatrix}^{-1}. \quad (15)$$

Now that, suppose the the remote observer will point the telescope to a sky object with equatorial coordinates of δ and α at time t , the parameters L , M , and N will be obtained from Eq. 16, then Eq. 17 will give the output of l , m , and n . Finally, the horizontal coordinates of the acquired sky object are calculated from Eqs. 18 and 19.

$$\begin{bmatrix} L \\ M \\ N \end{bmatrix} = \begin{bmatrix} \cos \delta \cos \alpha - k(t - t0) \\ \cos \delta \sin \alpha - k(t - t0) \\ \sin \delta \end{bmatrix}. \quad (16)$$

$$\begin{bmatrix} l \\ m \\ n \end{bmatrix} = T \begin{bmatrix} L \\ M \\ N \end{bmatrix}. \quad (17)$$

$$\phi = \tan^{-1}(m/l). \quad (18)$$

$$\psi = \sin^{-1}(n). \quad (19)$$

Eventually, the authors integrated the data of HC communication protocol with the extracted packets using reverse engineering to create a custom computer program for the telescope. This interface access all aspects of mount functions, including home position setting, last alignment process, and remote pointing correction.

TABLE 4. Focus controller communication.

Pin No	function	Type
02	Focus in remotely with certain value	Output
03	Focus out remotely with certain value	Output
04	Focus in remotely	Output
05	Focus out remotely	Output
06	Stop motion remotely	Output
07	Sense focus in limit switch	Input
08	Sense focus out limit switch	Input
09	Sense home position limit switch	Input
10	TX Wireless Module (RF)	
11	RX Wireless Module (RF)	
12	Sense focus in bush button	input
13	Sense focus out bush button	Input
A0	Stepper motor Pin A+	Input
A1	Stepper motor Pin A-	Output
A2	Stepper motor Pin B+	Output
A3	Stepper motor Pin B-	Output
A4	LCD	
A5	LCD	

B. FOCUS SYSTEM DEVELOPMENT

Indisputably, the focus significantly affects the quality of the astronomical observations, therefore it should be performed precisely [45]. As described before, the more risky part of the previous focus mechanism is that it has no physical feedback as it has been designed for human intervention operations. Therefore, the observer should have adequate experience to detect the limits in the two directions of the focus motion. Furthermore, it restricts the focus range with an estimated range regardless of the real focus range available despite the long travel necessary for observing [46].

The proposed integrated control system has been designed based on a ULN2003A driver for the stepper motor combined with an Arduino controller. Arduino is a re-programmable open-source micro-controller, an inexpensive computing platform that creates an interactive environment with devices and sensors [47]. Moreover, it is efficient in practical implementation, particularly in robotic projects [48]. This modified control system provides manual and computerized operation with LCD for focus position monitoring. Moreover, physical feedback is implemented via three limit switches relevant to mirror motion. Table 4 illustrates the configuration of the controller pins and their functions to adjust the focus remotely with adequate accuracy and safely via a graphical interface that gives all information about the position and switches. The control system in the architecture shown in Fig. 3 manages all switches, the LCD, and the wireless communication. It provides a programmed switching sequence to the stepper motor driver. The focus controller communicates wireless with the central control unit to avoid slipping cables out from their connector after repeated movement of the telescope [49]. It has been established using a 433MHz wireless serial radio frequency (RF) module that based on the Universal Asynchronous Receiver/Transmitter (UART) technology.

C. DOME AUTOMATION

The dome rotation was driven manually through push buttons without digital feedback; nevertheless, the shutter’s power

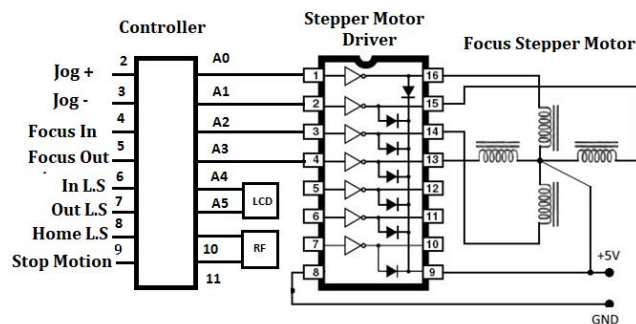


FIGURE 3. Implemented focus control unit.

feeding exhibited the most challenging issue. The electric source is fixed at the concrete wall that carries the dome; meanwhile, the shutters are rotated with the dome. So that the observer has to connect its cables manually to the nearest outlet in the wall to power the dome slit; after that, he opens the shutters completely, then plugs the cables off to start observation and repeats this sequence after finishing the observation. As a result, the dome automation starts with designing an electric mechanism that feeds the shutters automatically.

Standard solutions for supplying rotated objects with electric power from a fixed electric source are represented in two techniques. The first is a complete solar cell system with a battery mounted above the dome from outside with wireless communication for signals [49]. Another solution is a set of circular electric conductor bars named slip rings mechanism with carbon brushes that transfer power to the shutters where signals are transferred through wires [50]. These two traditional solutions are not affordable, need excessive maintenance, and are risky. So that our modified technique takes part of the second solution based on the electric conductor as indicated in Fig. 4; however, it is inexpensive and prevents any risk probability. It comprises two platforms; one is fixed and has the electric source, while the other is rotated with the dome body. Fig. 4(a) depicts the power platform construction where the fixed one includes a spring at its base point for smooth contact and flexibility. It also contains a limit switch to determine the dome’s home position. Meanwhile, the rotated one is routed directly to the shutters unit and isolated perfectly.

The technique concept is shown in Fig. 4(b); at the dome’s home position determined by a limit switch, the two platforms are aligned together and contacted. In case of the need to handle the shutters manually, the observer can use one bush button, which will rotate the dome to its home position to transfer power to the shutters. After the open process is completed, the power is switched off automatically, and this procedure is repeated when the observation is finished. After that and based on the Arduino controller, a control system has been implemented for the remote operation of dome rotation and shutters units. Moreover, there is a wireless HC for in-site observation and attended maintenance. A sample from control units designed and implemented for the observatory appears in Fig. 5 relative to the shutters. Fig. 5(a) shows the

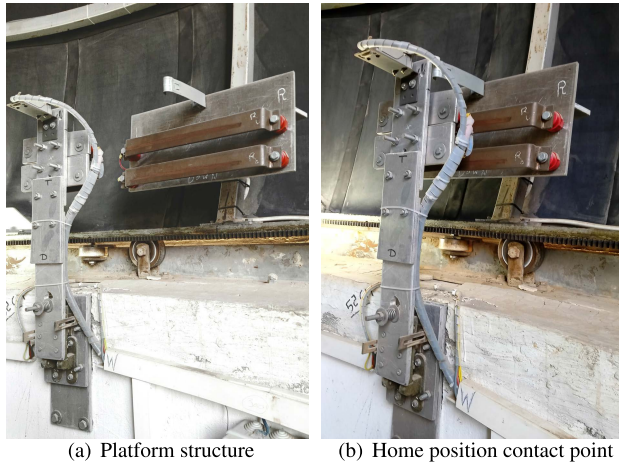


FIGURE 4. Electric power platform for feeding the shutters.

internal connection of the controller embedded circuit where the controller itself is fixed on the back side of the main card. In order to insulate the controller from the high current of motors, an intermediate control circuit has been designed based on switching relays as Fig. 5(b) presents. Since the dome is represented the core of an astronomical observatory, its remote control system should be robust with a convenient response to provide reliability, and safe [51]. The dome position, named dome azimuth (φ), is monitored through an incremental encoder installed on the rotating dome, and its position is calculated by converting digital pulses of the encoder into angular values as in Eq. 20.

$$\varphi = \frac{360 * (\text{number of applied pulses})}{(\text{total pulses per one revolution of the dome})}. \quad (20)$$

Dome synchronization is a crucial process in observation; it means positioning the dome slit at a specific angular point aligned with the telescope’s optical axis to provide sight to the sky [52]. Auspiciously, our telescope mounts support base is established at the center of the dome; subsequently, the φ is equal to the telescope azimuth (ϕ), referring to Eq. 21 [53].

$$\varphi = \phi + \sin^{-1} \left(\frac{d * \sin(\phi - 255)}{R} \right), \quad (21)$$

where R is the dome diameter, and d is the shift between the dome and telescope mount centers. Nevertheless, with time, an accumulated error will produce a slight shift in synchronization as a reason for mechanical coupling. Therefore, the control system automatically senses four limit switches around the dome diameter to correct this error and accurately maintain the dome slit synchronized with the telescope.

In order to guarantee extra protection against any occasional fault during remote observation, mechanical limit switches detect complete closing and opening. In addition, a time interval restricts each motion in the dome; if the time exceeds, the controller gives a remote alarm and stops the motor to avoid any damage.

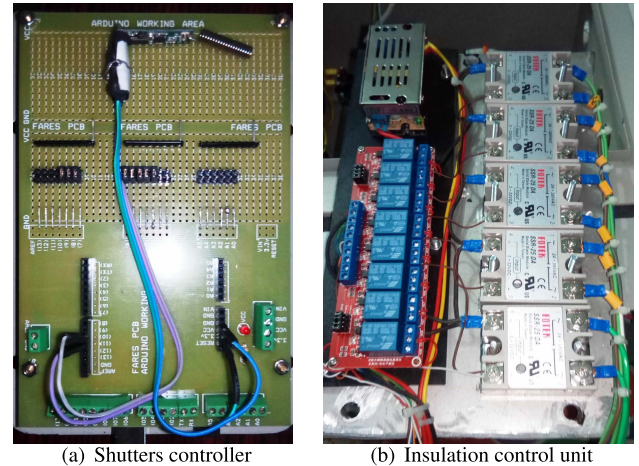


FIGURE 5. Shutters control unit.

D. CCD CAMERA PROCESSING

STX-16803-SBIG CCD camera is used in our developed observing platform; it has a USB and Ethernet connection. Besides, the SBIG FW7-STX filter wheel is equipped with the camera via the I^2C protocol. The hypertext transfer protocol (HTTP) allows the STX camera to be accessed across various PC platforms without any special driver requirements using a commands in [54]. Based on this document, the authors have created a GUI interface that provides all available aspects controlling the STX. The observer can take a scientific or guiding image and get information about the camera and filter wheel. The acquired images are compressed and sent to the remote observer. In addition, he can change the image header parameters, such as the observer and object names.

E. CONTROL SYSTEM OVERALL LAYOUT AND COMMUNICATION

Fig. 6 depicts a schematic diagram for the overall system of the 14-inch observatory. The remote observer communicates the dome server via a peer-to-peer (P2P) socket-based TCP-IP protocol. The P2P is a network communication architecture currently considered an efficient technique for allowing data transmission between custom software [55]. A router with a subscriber identification module (SIM) provides the observatory with the internet. This SIM includes a real IP address to enable access from all over the world. The dome server is a personal computer (PC) installed inside the dome and connected directly with all the observatory devices through three communication protocols, RS-232 protocol for the telescope and USB for both dome units master and focus system. Meanwhile, the SBIG and monitoring cameras are connected via the ETHERNET protocol. The monitoring cameras consist of two movable web cameras with infrared (IR) to quickly check the dome and devices inside the observatory as it is necessary for remote observation [52].

It is evident that occupying all PC ports reduces the efficiency of operation; thus, the master unit handles all dome

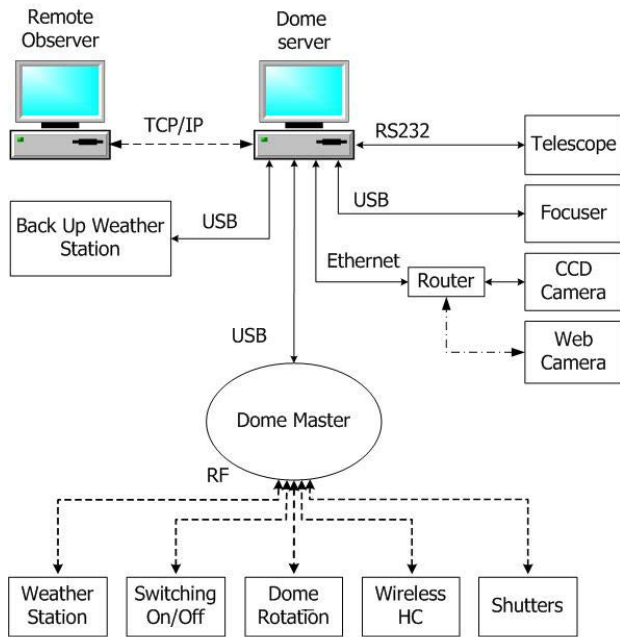


FIGURE 6. Observing control system block diagram.

control units wireless via RF. This modified master control unit handles commands and responses between the server and all dome instruments, such as dome rotation, shutters, wireless HC for inside dome operation, a switching control unit to enable remote switching of all devices on/off, and a weather station. The design of these units is similar to the shutters unit based on the Arduino controller and embedded systems. Since the weather information significantly impacts the observatory protection [36], a weather station named Davis Vantage pro2 [56] has been utilized. It has two ways to access information; one is through commercial software; another is via a serial communication protocol based on raw packets, which our interface depends on it [57]. In addition, another custom weather station based on sensors for temperature, humidity, wind speed, and rainfall has been designed and inserted as a backup in case of failure to avoid any weather damage [58]. Data transmission between the dome server and the other control units concerning the dome is based on the dome master unit. It receives data dome from the dome server and then sends it to the appropriate unit and transmits responses to the dome server. The communication procedure has been designed to guarantee the proper transfer of data between the master controller and other control units. As each unit has a specific ID, the master ID is MD, RD for dome rotation, WD for the weather station, HD for wireless HC, PR for the switching power unit, and SD for shutters unit. The message packet format is described in a specific sequence: message source, message destination, message data, message length, and message response. For instant, if the observer needs to rotate the dome in the right direction, the dome master command will be “MD, RD, RDR, 3, ACK,”. RDR means rotate the dome in the right direction, and ACK refers to the response type that does not contain information with

the response “RD, MD, OK, 3, ACK”. Meanwhile, if the command is to get information such as getting dome azimuth, the packet will be “MD, RD, GDZ, 3, INF” with the response of “RD, MD, 90, 2, INF”, as apparent the dome azimuth is 90 with a length of two characters.

F. GRAPHICAL USER INTERFACE (GUI)

The interaction design of GUI in this research relies heavily on written computer programs to avoid any restrictions related to the individual software of devices. Designing and implementing a custom GUI provides access methods for modification, keyboard shortcuts definition, and design interaction window for user [2]. The GUI application of the 14-inch CGE observatory is a single window covering all requirements for remote astronomical observing. It also exhibits visibility for the whole system with a fast display for the status of attached devices. Furthermore, it has an outstanding efficiency in making appropriate decisions in case of risk, such as closing the shutters automatically during lousy weather. Moreover, each motion in the observatory has a physical limit and time restriction, and if a motion exceeds its normal time, the system will detect a fault. This time limit is essential to protect motors and mechanical parts from damage in case of the failure of the limit switches. The GUI includes several modes of operation, such as remote and onsite, beside an engineering mode in order to overcome technical faults remotely. In the engineer mode, the remote technician could set and check critical parameters in case of technical tests, debugging and fault diagnosis. The remote technician has a significant facility for violating system limits and directly commanding the ports.

The GUI structure is eleven tabs, as shown in Fig. 7, which displays a screenshot from the GUI; each tab displays current information about the instrument besides a facility for controlling it. Primarily, this figure focuses on two essential tabs, a telescope pointing window and a soft buttons for the dome. The telescope tab depicts the local and the world time; moreover, it includes a catalog for some sky objects where the observer has a facility to select from them or enter another object’s coordinates. After selecting, all transformation and information of the object will be displayed before pointing. The soft buttons tab shows necessary information about the dome position and direction, shutters status and current weather station information. Furthermore, It displays a soft buttons with a full capability to control the dome rotation, shutters, switching devices and lights besides an emergency stop button.

IV. ADVANCED SIMULATION STUDY OF THE 14-INCH TELESCOPE FOR ENHANCING ITS PERFORMANCE

A. TELESCOPE MODEL OF 14-INCH TELESCOPE

The dynamical model of the telescope is represented in some differential equations with a nonlinear coupled type that includes a varying inertia term (M), Coriolis and centrifugal term (C), and gravity term (G). The (G) term tends to

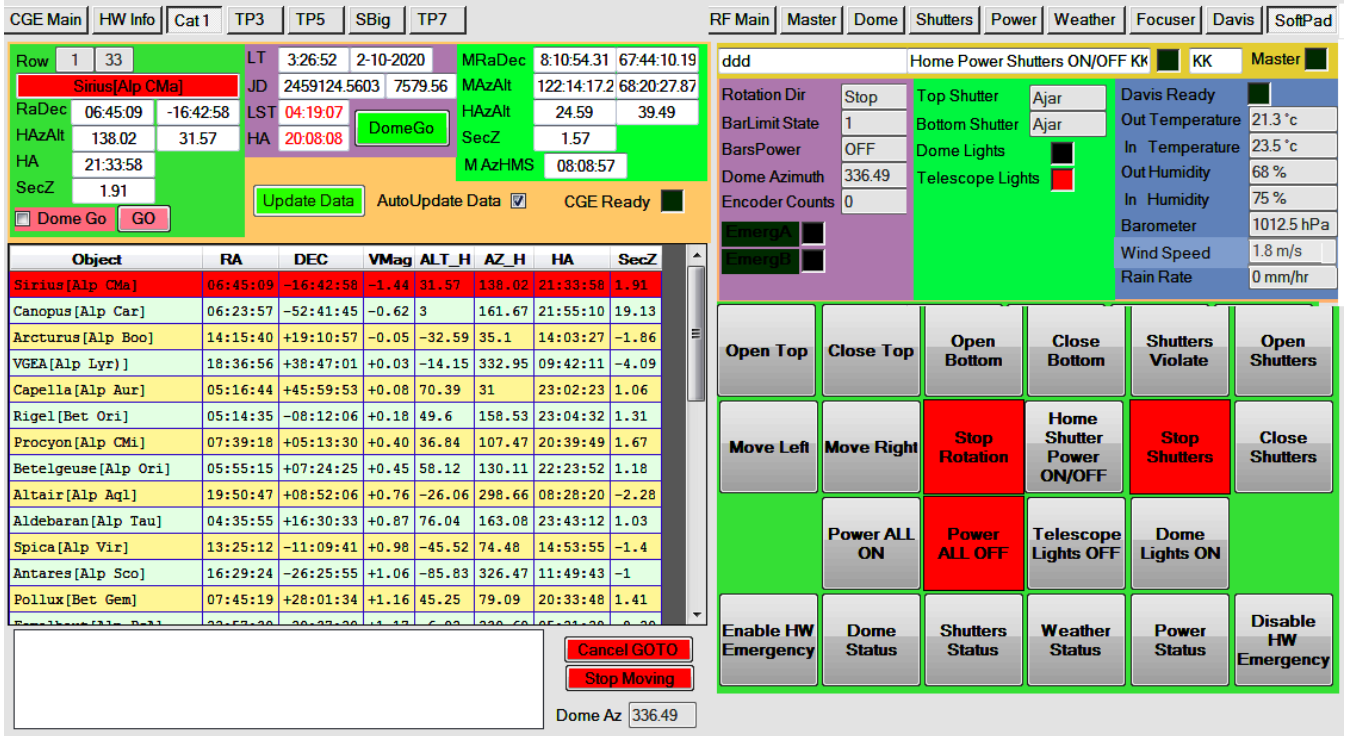


FIGURE 7. GUI screenshot of 14-inch telescope for remote observing.

zero in the case of an accurately balanced telescope and a frictional term (N). It has been designed upon an assumption of ignoring the friction at the telescope joints as in Eqs. 22, and 23 [22].

$$M(\theta)\ddot{\theta} + C(\theta, \dot{\theta}) + G(\theta) = \tau, \quad (22)$$

$$M(\theta)\ddot{\theta} + N(\theta, \dot{\theta}) + \tau_d = \tau, \quad (23)$$

where θ , $\dot{\theta}$, and $\ddot{\theta}$ are respectively the joint angular term of position, velocity, and acceleration. Meanwhile, τ is the input joint torque, and τ_d is the disturbance torque. The telescope model includes two main input torques τ_1 and τ_2 in two directions, RA and DEC, with two angular positions θ_1 and θ_2 in the output as shown in Eq. 24. Equations of inertia matrix, Coriolis and centrifugal torque, and the Gravity term are described in detail in [22].

$$\theta = \begin{bmatrix} \theta_1 \\ \theta_2 \end{bmatrix}, \quad \dot{\theta} = \begin{bmatrix} \dot{\theta}_1 \\ \dot{\theta}_2 \end{bmatrix}, \quad \ddot{\theta} = \begin{bmatrix} \ddot{\theta}_1 \\ \ddot{\theta}_2 \end{bmatrix}. \quad (24)$$

The 14-inch telescope model is a coupled system; therefore, it has decoupled by inserting a compensator, and as a result, a decoupled system can be thought of as a collection of autonomous single variable systems to produce a linear system for enabling different controllers to be used in controlling the telescope response [59]. The entire input torque for the telescope's nonlinear model is made up of a compensator fed from two parallel controllers signals, where the state variables (θ_1 , θ_2 , $\dot{\theta}_1$, and $\dot{\theta}_2$) are processed by a controller that consists of a state feedback compensator and a linear controller [21]. Authors of [22] have gone over in-depth the equations of the compensator.

The linearized model comprises the nonlinear telescope model and the compensator is depicted in Fig. 8, where U_1 and U_2 are the controller outputs that will feed the compensator; meanwhile, the output of the compensator reveals to the input joint torques. The state variables will be returned to the compensator then the output positions will be the actual feedback signals to the controllers for RA and DEC, respectively.

B. PROPOSED ID-T AND TID CONTROLLERS

FO concept is based on the expansion of integer order integration and differentiation to a fractional order operator. FO calculus-based controllers such as TID are utilized frequently due to their improved capacity to reject disturbances and higher sensitivity to changes in model parameters [60]. TID controller is similar to the PID structure; however, the proportional component is replaced by a tilted component $1/s^{1/n}$ to produce a transfer function described in Eq. 25 [61].

$$u(t) = \frac{K_T}{s^{1/n}} + \frac{K_I}{s} + K_D s, \quad (25)$$

where K_I , K_D , and K_T express the proportion coefficients, integral coefficients, and proportional component tilt gain, respectively. At the same time, n is represented as a fractional-order positive parameter in the range of 1 to 10. Block diagram of the TID controller is shown in Fig. 9 where the coefficients take a direction of feed-forward to ensure ease tuning as well as optimal response approach beside better sensitivity to parametric variations of the system [62]. The input parameter $r(t)$ refers to a reference set value, while

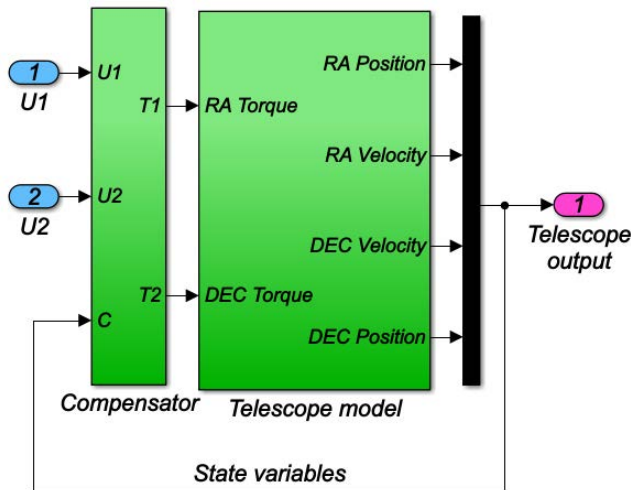


FIGURE 8. Telescope linear model.

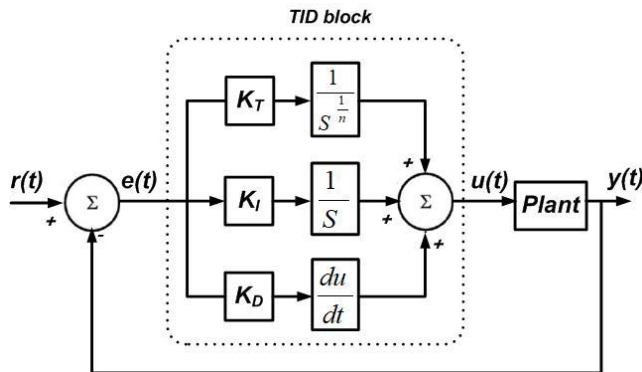


FIGURE 9. TID block diagram.

$u(t)$ represents the controller’s output. The error $e(t)$ is the estimated difference among $r(t)$ and actual output of a plant $y(t)$. On the other hand, ID-T is a modified version of the TID, whereas the tilt parameter takes the feedback direction as Fig. 10 depicts. Furthermore, a derivative filter is inserted in the ID-T controller, which can be set in the range of [1, 500] [63]. This modified FO controller has been designed mainly for the power system-related load frequency control issues due to its capability to minimize the O_{sh} time. The distinguishing characteristics of the ID-T give a definite prediction of its efficiency in enhancing the telescope performance. The ID-T mathematical design is represented in the transfer function appeared in Eq. 26 [31].

$$u(t) = \left(\frac{K_I}{S} + K_D \frac{N_C}{1 + N_C (1/S)} \right) e(t) - \left(\frac{K_T}{S^{1/n}} \right) y(t). \quad (26)$$

C. PSO AND PROPOSED POA ALGORITHMS

Utilized PSO parameters coefficients are illustrated in Table 5; however, all mathematical details of PSO are described briefly in [64].

The POA is inspired by the behaviors and living habits of a bird named peafowl; their male has extravagant feathers and harsh calls and is referred to as peacock; meanwhile, the female is called peahens. Mating and food searching are the

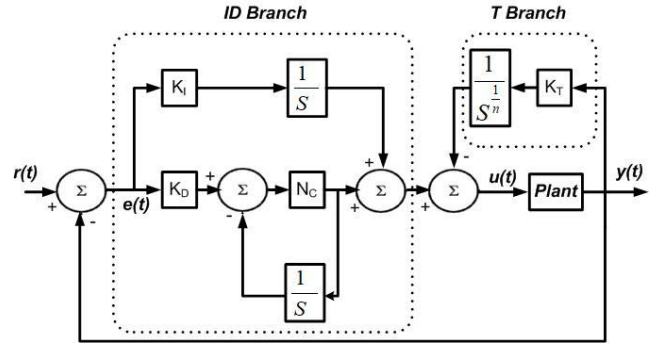


FIGURE 10. ID-T block diagram.

TABLE 5. PSO parameters.

Maximum number of iterations	50
Particles number (swarm size)	20
Inertia coefficient	1
Damping ratio of inertia coefficient	0.99
Personal acceleration coefficient	2
Social acceleration coefficient	2

most significant aspects of this type of swarm, in which the POA algorithm is built.

Establishing a mathematical model efficiently for a peafowl swarm requires dividing it into three groups, the first is the adult peacock, the second is adult peahens, and the third group is peafowl cubs. In real-world optimization issues, every peafowl is rated according to its fitness value, and initially, there are five solutions, starting with peacock one and ending with peacock five, respectively. Furthermore, the first remainder, 30% of individuals, is classified as adult peahens, while the rest are classified as peafowl cubs. Immediately after finding a food source by peacocks, they will rotate around it to show off and attract peahens as a way to mate. The show is represented in tail spreading with dancing behavior, flapping feathers producing attractive sounds, and rotating around peahens that have been approached.

Converting peacock behaviors into an appropriate mathematical model is primarily based on their rotation aspects, leading to their fitness estimation during iterations. Peacocks with a higher fitness mark are more likely to circle the food source with a smaller circle radius, whereas those with a lower fitness value are more likely to spin in site with a broader circle radius. During the whole seeking process, peahens use an approaching mechanism and an adaptive searching to dynamically change their behaviors at various phases. The peacock’s fitness rating indicates the likelihood of attracting a peahen. Peafowl cubs serve as seeking agents, randomly exploring for the best-quality food source in the searching region in a Levy flight distribution, in addition to approaching male peacocks with good food sources with a high fitness value, one of the assumed five peacocks. As a result, the four peacocks will go toward the selected peacock in a random path within 90 degrees of the line between peacock one and the other, as shown in Fig. 11.

Only when the respective peafowls' fitness is improved, their placements are modified and updated immediately after executing the above four peafowl behaviors (namely, peacock courtship behaviors, peahen adaptive approaching behaviors, peafowl cubs adaptive searching behaviors, and interaction behaviors among peacocks). Each peacock is impacted directly or indirectly by Peacock one, which has the most fantastic current fitness value, ensuring POA convergence, avoiding early convergence, and settling for a local optimum. POA will keep the current best solution, and instead of remaining motionless, the five mentioned peacocks, which represent the current ideal solutions, will hunt throughout the surrounding searching space using a rotating dance mechanism. During iterations, peahens are interested in local exploitation in the early stage of the iteration and tend to elaborate more focus on global exploration in both the middle and behind the stage, whereas peafowl cubs perform in reverse order, which can successfully complement each other. As a result, both local and global explorations are achieved throughout the iteration, thereby improving the efficiency and quality of the optimization [32]. The fitness evaluation is based on the circle radius; the best will circle around the source of the food in a smaller radius; however, a larger radius in rotation tends to have poor fitness value as represented mathematically in Eqs. 27 -32.

$$X_{Pc1} = X_{Pc1}(t) + R_s \cdot \frac{X_{r1}}{\|X_{r1}\|}, \quad (27)$$

$$X_{Pc2} = \begin{cases} 1.5 \cdot X_{Pc2}(t) + R_s \cdot \frac{X_{r2}}{\|X_{r2}\|} & r2 < 0.9 \\ X_{Pc2}(t) & \text{otherwise,} \end{cases} \quad (28)$$

$$X_{Pc3} = \begin{cases} 2 \cdot X_{Pc3}(t) + R_s \cdot \frac{X_{r3}}{\|X_{r3}\|} & r3 < 0.8 \\ X_{Pc3}(t) & \text{otherwise,} \end{cases} \quad (29)$$

$$X_{Pc4} = \begin{cases} 3 \cdot X_{Pc4}(t) + R_s \cdot \frac{X_{r4}}{\|X_{r4}\|} & r4 < 0.6 \\ X_{Pc4}(t) & \text{otherwise,} \end{cases} \quad (30)$$

$$X_{Pc5} = \begin{cases} 5 \cdot X_{Pc5}(t) + R_s \cdot \frac{X_{r5}}{\|X_{r5}\|} & r5 < 0.3 \\ X_{Pc5}(t) & \text{otherwise,} \end{cases} \quad (31)$$

$$X_r = 2 \cdot \text{rand}(1, \text{DIM}) - 13, \quad (32)$$

where X_{Pci} stands for the i th male peacock's position vector, $i = 1, 2, \dots, 5$; while R_s represents the rotation radius during circling around; whereas, X_r refers to a random vector. $\|X_r\|$ is the X_r modulus, while Dim is represented the variable's numbers. Besides, the radius of rotation R_s is designed to dynamically change with iterations, which is estimated as

$$R_s(t) = R_{s0} - R_{s0} \cdot (i/i_{max})^{0.01}, \quad (33)$$

where i and i_{max} represent the current iteration's number and the maximum number of iterations. While R_{s0} stands for the vector of the radius of initial rotation and is calculated from Eq. 34 based on lower bounds (LB) and upper bounds (UB)

of the unknown parameters.

$$R_{s0} = 0.2(\text{UB} - \text{LB}). \quad (34)$$

The mathematical model that describes behaviors of peahens and the approaching mechanism is represented in

$$X_{Ph} = \begin{cases} X_{Ph}(t) + 3 \cdot \mu \cdot (X_{Pc1} - X_{Ph}(t)), & 0.6 \leq r_5 \leq 1 \\ X_{Ph}(t) + 3 \cdot \mu \cdot (X_{Pc2} - X_{Ph}(t)), & 0.4 \leq r_5 \leq 0.6 \\ X_{Ph}(t) + 3 \cdot \mu \cdot (X_{Pc3} - X_{Ph}(t)), & 0.2 \leq r_5 \leq 0.4 \\ X_{Ph}(t) + 3 \cdot \mu \cdot (X_{Pc4} - X_{Ph}(t)), & 0.1 \leq r_5 \leq 0.2 \\ X_{Ph}(t) + 3 \cdot \mu \cdot (X_{Pc5} - X_{Ph}(t)), & 0 \leq r_5 \leq 0.1 \end{cases} \quad (35)$$

$$\mu = 1.1 - (0.1) \cdot (i/i_{max}), \quad (36)$$

where r_5 is a uniformly distributed random number in a range of [0,1] and X_{Ph} represents the peahens position vector. Despite the peacocks having a food source in a specific area, the peafowl cubs in a task as agents are searching randomly for a better food source in the space of searching. This searching is defined as a Levy flight that is described in detail in [65], where each peafowl cub has a specific behavior that modelled as:

$$X_{SPc} = \begin{cases} X_{Pc1}(t), & 0.8 \leq r_8 \leq 1 \\ X_{Pc2}(t), & 0.6 \leq r_8 \leq 0.8 \\ X_{Pc3}(t), & 0.4 \leq r_8 \leq 0.6 \\ X_{Pc4}(t), & 0.2 \leq r_8 \leq 0.4 \\ X_{Pc5}(t), & 0 \leq r_8 \leq 0.2 \end{cases}, \quad (37)$$

$$X_{PcC} = X_{PcC}(t) + \gamma \cdot \text{Levy}(X_{Pc1}(t) - X_{PcC}(t)) + \sigma \cdot (X_{SPc} - X_{PcC}(t)), \quad (38)$$

where r_8 refers to a uniformly distributed random number within [0, 1], while X_{SPc} and X_{PcC} denotes the peacock's position vector and peacock cubs, respectively. γ and σ are coefficient factors that dynamically change during iterations and are calculated as follows:

$$\gamma = 0.9 - (0.5) \cdot (i/i_{max})^2. \quad (39)$$

$$\sigma = 0.1 - (0.9) \cdot (i/i_{max})^{0.5}. \quad (40)$$

Interaction behaviors among peacocks start as peacock one has the best food source. The four remaining peacocks will be motivated to reach it in a random direction within 90 degrees of the line between peacock one and the others as shown in Fig. 11 with a mathematical relation as

$$\begin{cases} X_1 = X_{Pc1} - X_{Pc2} \\ X_2 = X_{r6} - \frac{X_{r6} * X_1}{X_1 * X_1} \cdot X_1 \\ X_{Pc2} = X_{Pc2}(t) + \mu \cdot X_1 + r_{09} \cdot \frac{X_2}{\|X_2\|}, \end{cases} \quad (41)$$

$$\begin{cases} X_3 = X_{Pc1} - X_{Pc3} \\ X_4 = X_{r7} - \frac{X_{r7} * X_3}{X_3 * X_3} \cdot X_3 \\ X_{Pc3} = X_{Pc3}(t) + \mu \cdot X_3 + r_{10} \cdot \frac{X_4}{\|X_4\|}, \end{cases} \quad (42)$$

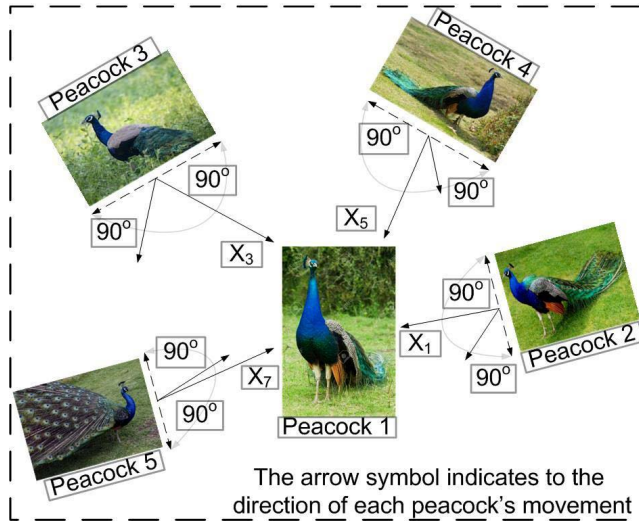


FIGURE 11. Mechanism for interactions between different peacocks.

TABLE 6. POA parameters.

Maximum number of iterations (i_{max})	50
Population size	20
Number of independent runs	10
Visibility factor of peacocks	0.2

$$\begin{cases} X_5 = X_{Pc1} - X_{Pc4} \\ X_6 = X_{r8} - \frac{X_{r8} * X_5}{X_5 * X_5} \cdot X_5 \\ X_{Pc4} = X_{Pc4}(t) + \mu \cdot X_5 + r_{11} \cdot \frac{X_6}{\|X_6\|}, \end{cases} \quad (43)$$

$$\begin{cases} X_7 = X_{Pc1} - X_{Pc5} \\ X_8 = X_{r9} - \frac{X_{r9} * X_7}{X_7 * X_7} \cdot X_7 \\ X_{Pc5} = X_{Pc5}(t) + \mu \cdot X_7 + r_{12} \cdot \frac{X_8}{\|X_8\|}, \end{cases} \quad (44)$$

where X_{r6} to X_{r9} are generated four random vectors get from Eq. 32, and r_9 to r_{12} are four uniformly distributed random numbers on $[0, 1]$. The above table exhibits a pseudo-cod of the POA equations while Table 6 describes the selected parameters for our application regarding POA.

D. SIMULATION PROCESS

Fig. 12 illustrates the executed simulation procedure carried out upon the telescope model utilizing a hybrid of the ID-T controller and POA. The figure shows the architecture of two ID-T controllers including ten gains in two directions; RA and DEC. Each controller has its own parameters represented in the reference position ($\theta_{ref,RA}$, $\theta_{ref,DEC}$), the actual position (θ_{RA} , θ_{DEC}), and the error ($e(\theta_{RA})$, $e(\theta_{DEC})$). Meanwhile, the net telescope error in Eq. 45 is utilized as an objective function.

$$Error = e(\theta_{RA}) + e(\theta_{DEC}). \quad (45)$$

Indeed, the choice of performance criterion is the most critical component in improving system performance to minimize the error between the desired and actual position angles for RA

Algorithm 1 POA Algorithm

- 1: Set POA parameters as Table 6 depicts.
- 2: Set initial rotation radius (R_{S0}) from Eq. 34 using LB and UB in Table 7.
- 3: Initialize position of peafowl population.
- 4: Assign roles based on fitness function in Eq. 45.
- 5: **FOR** $i := 1$ to i_{max} ,
- 6: update μ , γ , and σ via Eqs. 36, 39, and 40 respectively.
- 7: Evaluate X_{Pc1} , X_{Pc2} , X_{Pc3} , X_{Pc4} , and X_{Pc5} from Eqs. 27 -32.
- 8: **FOR** $k := 1$ to 5,
- 9: Inspect and correct X_{Pci} to be within a correct range.
- 10: **IF** X_{Pci} fitness is better than $X_{Pci}(t)$.
- 11: $X_{Pci}(t + 1) = X_{Pci}$.
- 12: **END IF**.
- 13: **END FOR**.
- 14: **FOR** $j := 1$ to number of peahens,
- 15: Calculate X_{Ph} using Eq. 35.
- 16: Inspect and correct X_{Ph} to be within a correct range.
- 17: **IF** X_{Ph} fitness is better than $X_{Ph}(t)$ fitness,
- 18: $X_{Ph}(t + 1) = X_{Ph}$.
- 19: **END IF**.
- 20: **END FOR**.
- 21: **FOR** $j := 1$ to number of peafowl cub,
- 22: Estimate X_{SpC} using Eq. 37.
- 23: Calculate X_{PcC} using Eq. 38.
- 24: Inspect and correct X_{PcC} to be within a correct range.
- 25: **IF** X_{PcC} fitness is better than $X_{PcC}(t)$ fitness,
- 26: $X_{PcC}(t + 1) = X_{PcC}$.
- 27: **END IF**.
- 28: **END FOR**.
- 29: Evaluate X_{Pc2} , X_{Pc3} , X_{Pc4} , and X_{Pc5} from Eqs. 41 -44
- 30: **FOR** $i := 2$ to 5,
- 31: inspect and correct X_{Pci} to be within a correct range.
- 32: **IF** X_{Pci} fitness is better than $X_{Pci}(t + 1)$ fitness,
- 33: $X_{Pci}(t + 1) = X_{Pci}$.
- 34: **END IF**.
- 35: **END FOR**.
- 36: Based on fitness reassign roles.
- 37: **END FOR**.

and DEC with achieving the best performance characteristics. Therefore, and because of its benefits in reducing settling time, the integral time absolute error (ITAE) is used as a performance criterion; meanwhile, the integral time square error (ITSE) based control structure generates a large output signal in response to an unexpected change in the reference signal [66]. Furthermore, the ITAE produces less overshoot and oscillations than the integral-of-the-absolute error (IAE) and integral-of-the-square error (ISE). The applied ITAE objective function in Eq. 46 is to achieve the optimal controller parameters for optimizing the fundamental telescope characteristics like maximum O_{sh} , R_s and T_s [67].

$$ITAE = \int_0^{\infty} |e(t)|d(t). \quad (46)$$

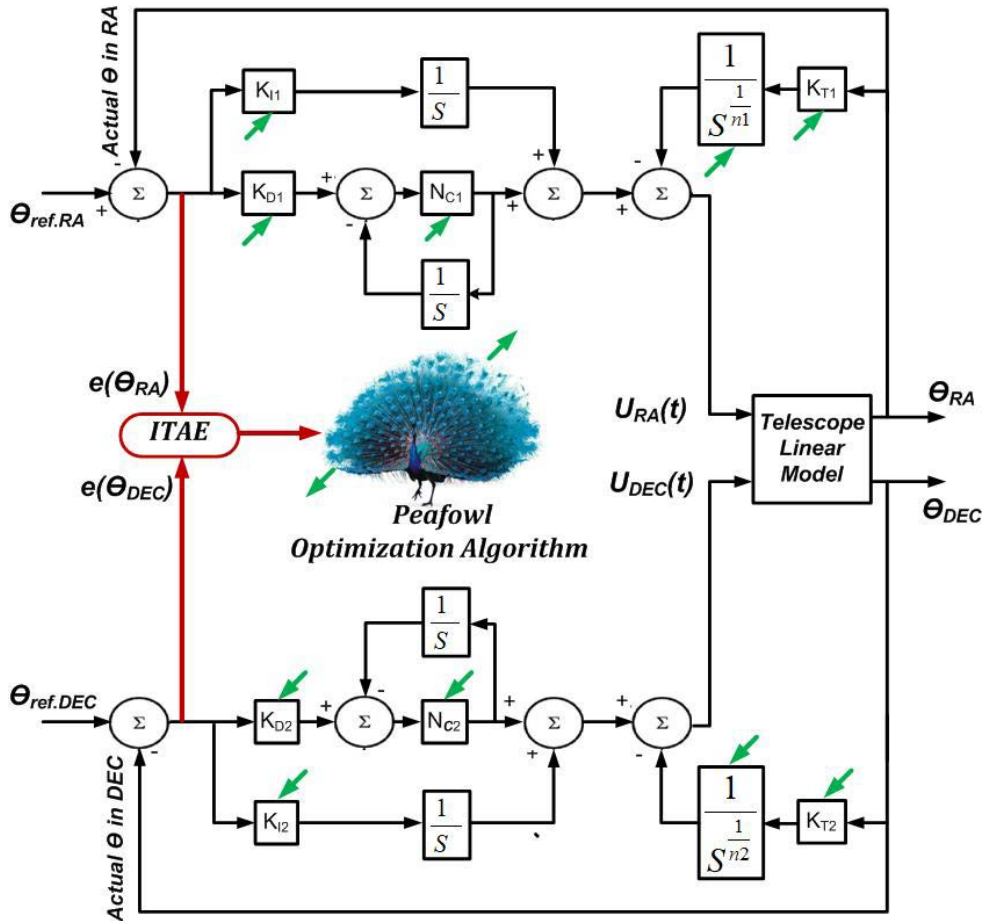


FIGURE 12. Block diagram of the telescope model including the ID-T controller based POA.

TABLE 7. Unknown parameters range.

	TID				ID-T				
	K_T	K_I	K_D	n	K_T	K_I	K_D	N_C	n
LB	0	-10	-50	1	-1	-5	-50	100	1
UB	100	10	50	10	1	5	50	500	10

The gains limits of TID and ID-T controllers are established and determined classically as in Table 7 through extensive trial and error procedures based on a suggested tuning procedure in [68] and [69]. In the beginning, K_I and K_D are set to zero, whereas K_T is increased until reaching the minimum steady-state oscillation. After that, K_D is changed until the overshoot vanishes, while K_I is adjusted around zero until reaching a minimum rise time without any overshoot. Concerning n and N_C , they are limited, as mentioned before, from [0 10] and [0 500], respectively; however, it has been found empirically that the minimum limit of N_C is 100 has achieved considered performance. These values will be the boundary conditions for optimization for both PSO and POA.

V. RESULTS AND DISCUSSIONS

An overall view of the 14-inch observatory is shown in Fig. 13 represented in the telescope, which is considered the

core of observation attached by the SBIG camera, the filter wheel, and the focus motor. The figure also reveals the dome rotation unit; it comprises a controller cabinet provided by bush buttons and an emergency stop for in-site operation. The controller box, which is responsible for the dome rotation and transfers power to the shutters unit, is fixed on the left of the control cabinet. Moreover, the box on the right side comprises a three-phase inverter drive to adjust the rotation speed. All mentioned units are connected together in a wire form; meanwhile, they communicate with the server PC wireless.

A sky’s brightest star named Pollux in Fig. 14 has been observed remotely using the modified CGE control system; however, it has a shift, as shown in Fig. 14(a). By applying the procedure of remote pointing correction, the star has been approximately centered in the middle of the frame, as represented in Fig. 14(a).

Adjusting the focus of sky objects is essential to provide an adequate resolution; therefore, Fig. 15 confirms how the observer can focus celestial images remotely. Fig. 15(a) shows an observed frame with unfocused stars that appear stretched. Meanwhile, Fig. 15(b) reveals better resolution-focused stars with less size and higher quality.

Concerning the issue of dome automation cost, including control unit, software, and weather monitoring, the study

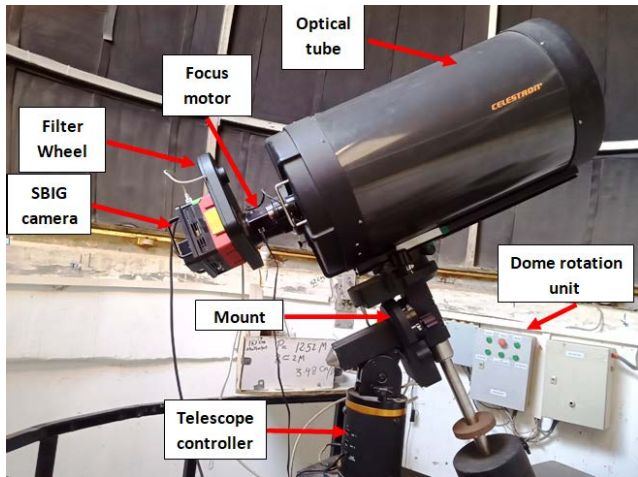


FIGURE 13. The 14-inch CGE telescope with attached devices and dome rotation control unit.

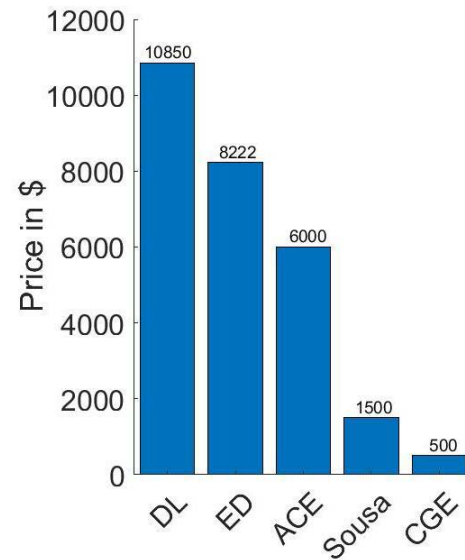


FIGURE 16. Dome automation cost in American dollars for commercial companies and past research.

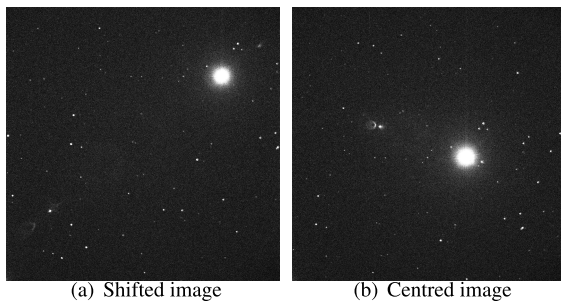


FIGURE 14. Observed Pollux star with automatic remotely centering using coordinates transformation procedure.

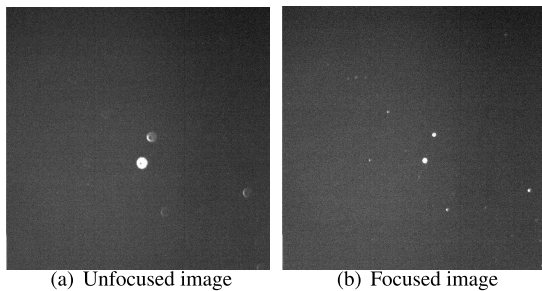


FIGURE 15. Observed sky image before and after the remotely focusing adjustment.

in [19] has mentioned two commercial companies shown in the bar chart in Fig. 16. One of them is Diffraction Limited (DL), with a budget of \$10850, while the other is Explore Dome (ED) is \$8222; meanwhile, there is a third company named Astronomical consultants and equipment (ACE) which automates astronomical domes for a price of \$6000. In addition, authors in [19] have performed a theoretical estimation for the dome automation budget with \$1500. Indisputably, the dome automation cost based on companies is so expensive compared with our implemented platform, which evaluated at \$500 under the name of CGE.

Regarding the simulation section, the data in Tables 8, 9 and 10 depict the results that have been employed with the MATLAB 2019a platform in an Intel core TM i7- 6500U

CPU, 8 GB RAM Laptop. The telescope system is built with MATLAB-SIMULINK, whereas POA and PSO codes are implemented in m files interfacing with the Simulink telescope model to optimize the process. Tables 8 and 9 show the coefficients optimized values of the TID and ID-T controllers, which have been obtained based on POA, PSO, and classical tuning. These values have resulted in the best performance of the telescope system by minimizing the times of settling and rising beside removing oscillations, as Table 10 reveals. The proposed ID-T controller optimized by POA has produced values as 0.1099 and 0.2050 seconds for R_s and T_s in the RA direction. The ID-T tuned by PSO has followed it with a little difference in the longer time for rising and settling. Although the TID output has small values as 0.0614 and 0.1796 seconds for R_s and T_s in the same direction, it is inconvenient due to the produced O_{sh} as of 2.7568 and 5.4947 seconds in POA and PSO, respectively. Meanwhile, classical tuning for both controllers has produced poor performance, particularly in R_s which reached 2.0512 and 1.3137 seconds in TID and ID-T.

Fig. 17 depicts the performance investigation of the telescope position and velocity responses in the RA direction with a reference angle position is 50 degrees. It is observed from Fig. 17(a) that the characteristics achieved by the ID-T controller are better than the TID. On the other hand, the TID controller performance has produced an O_{sh} by executing both algorithms POA and PSO; however, the O_{sh} is less in the case of POA. Regarding classical tuning for the two controllers, although the O_{sh} is zero, the consumed time to track the desired position with stability is long.

Simulation results concerning the variations of the velocity in the arms of RA are revealed in Fig. 17(b). The figure illustrates that the velocity generally tends zero immediately after reaching the desired position. The consumed time in the case of the TID-based PSO and POA is short; however, it generates some oscillations due to the O_{sh} produced before stability.

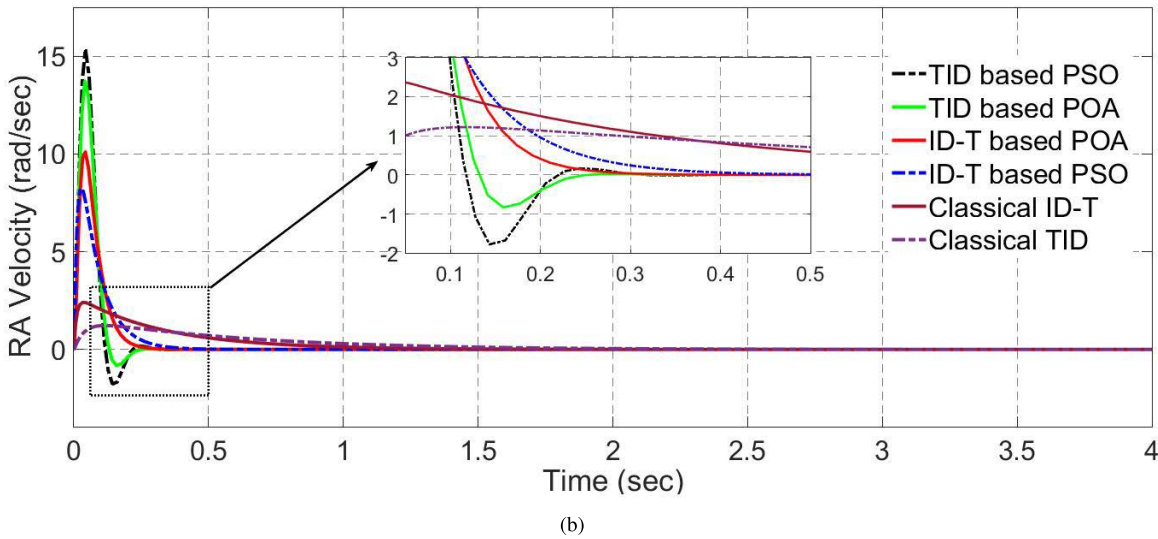
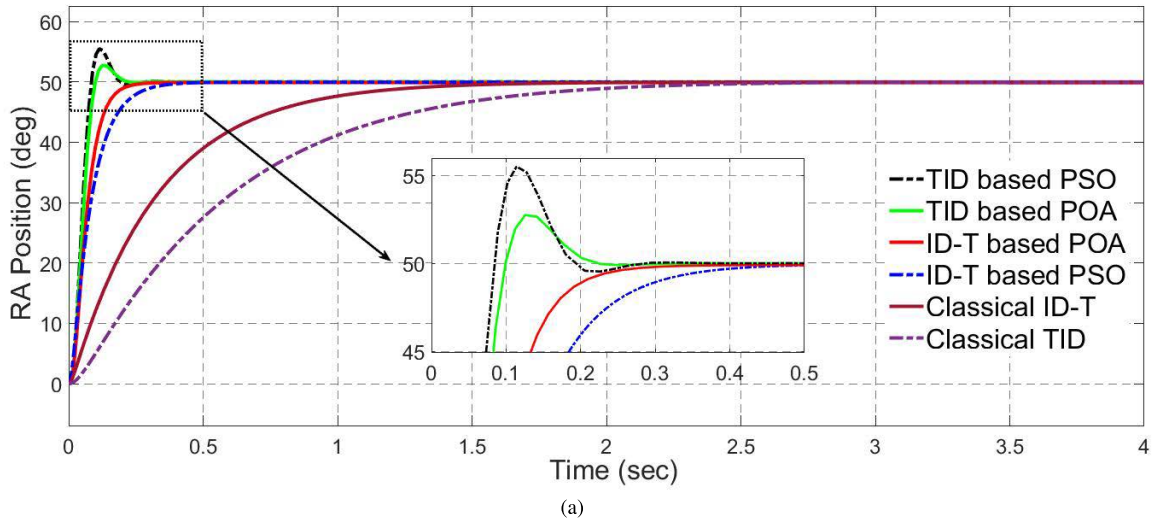


FIGURE 17. RA responses. (a): Position. (b): Velocity.

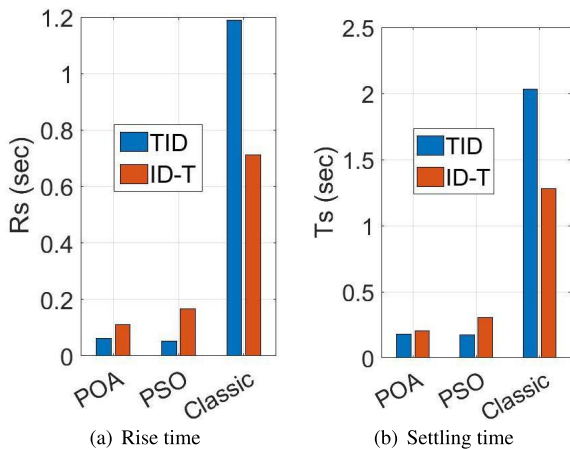


FIGURE 18. Bar chart comparing the performance of utilized controllers in terms of R_s and T_s in RA direction.

In contrast, the ID-T optimized via POA has tended to zero fast to achieve a stable performance without any oscillations,

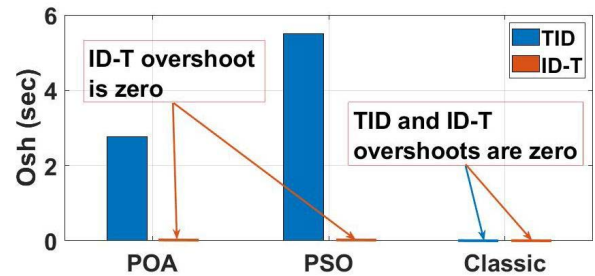


FIGURE 19. Bar chart comparing the performance of utilized controllers according to O_{sh} in RA direction.

followed by the ID-T-based PSO. Both controllers consume a long time for stability without oscillations, in the case of classical tuning.

The bar chart in Fig. 18 compares the characteristics and performance of the different utilized controllers-based optimization in the RA direction. It is apparent from the

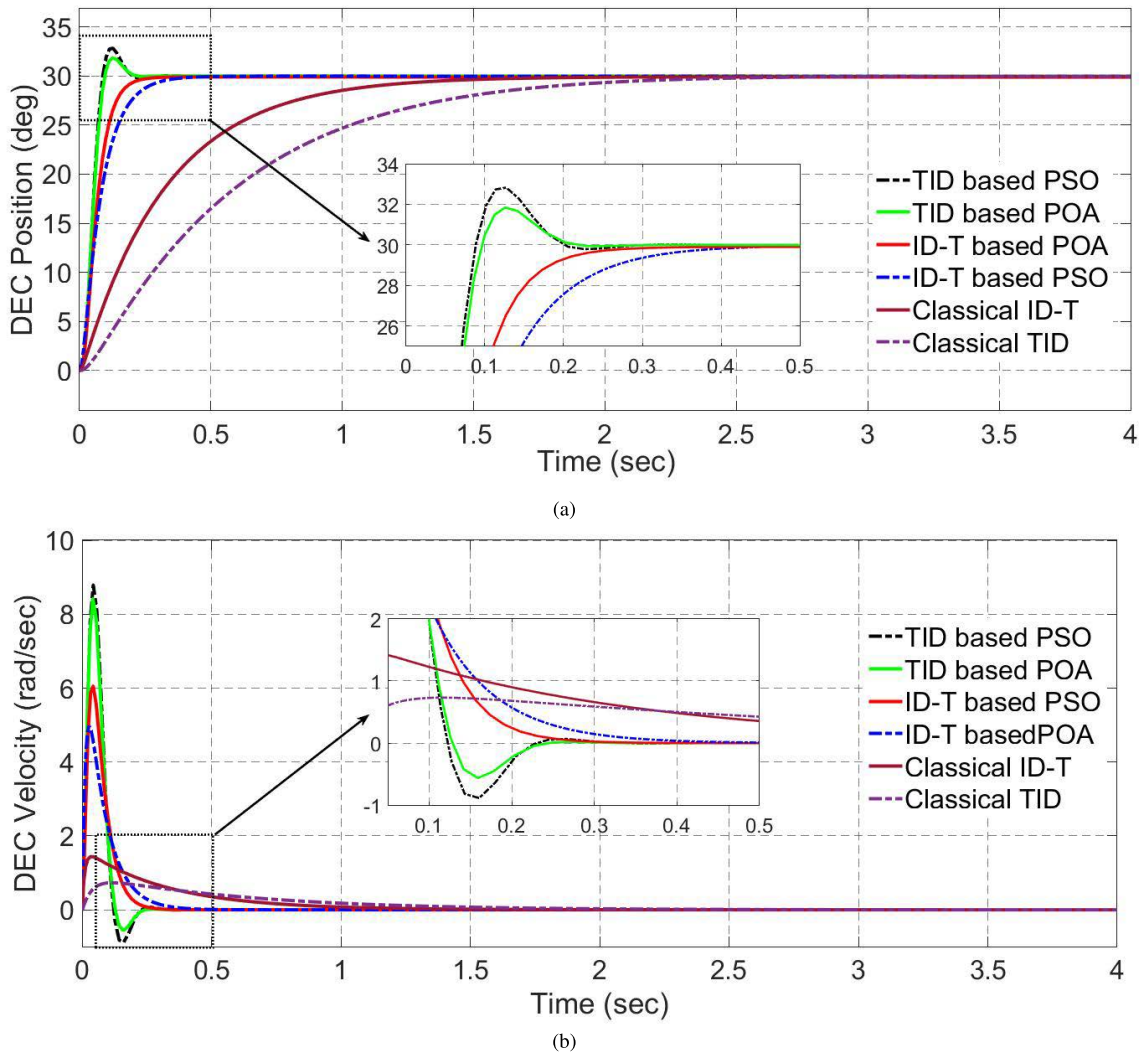


FIGURE 20. DEC responses. (a):Position. (b): Velocity.

TABLE 8. TID gains.

	RA				DEC			
	K_{T1}	K_{I1}	K_{D1}	n_1	K_{T2}	K_{I2}	K_{D2}	n_2
POA	70.15	-4.71	44.13	9.82	50.07	-7.26	35.24	8.25
PSO	37.17	-6.02	23.41	4.27	40.35	-3.52	43.18	2.76
Classic	50	-0.8	40	8	66	-0.6	33	4.2

TABLE 9. ID-T gains.

	RA					DEC				
	K_{T1}	K_{I1}	K_{D1}	N_{C1}	n_1	K_{T2}	K_{I2}	K_{D2}	N_{C2}	n_2
POA	0.22	2.19	48.81	449.44	8.56	0	1.23	32.17	330.29	3.35
PSO	0.02	0.97	33.39	419.53	7.96	0.55	0.3	24.95	357.32	8.27
Classic	0.5	3	13	450	9	0.56	7	13	340	6.5

figure that R_s and T_s in the TID are always smaller than ID-T except in classical tuning. However, the TID often produces an O_{sh} except during classical tuning, and it is a significant obstacle in observation other than the ID-T,

which produces zero O_{sh} persistently, as shown in Fig. 19. In conclusion, the proposed ID-T controller-based POA has exhibited an appropriate enhancement for the 14-inch CGE telescope.

TABLE 10. Performance results.

	TID			ID-T		
	POA RA - DEC	PSO RA - DEC	Classic RA - DEC	POA RA - DEC	PSO RA - DEC	Classic RA - DEC
R_s	0.0614 - 0.0600	0.0523 - 0.0558	1.1879 - 1.1920	0.1099 - 0.1104	0.1659 - 0.1658	0.7109 - 0.7170
T_s	0.1796 - 0.1777	0.1739 - 0.1786	2.0315 - 2.0512	0.2050 - 0.2077	0.3049 - 0.3049	1.2795 - 1.3137
O_{sh}	2.7568 - 1.8419	5.4947 - 2.8240	0 - 0	0 - 0	0 - 0	0 - 0

The simulation results of the DEC direction are shown in Fig. 20 with a reference position of 30 degrees. The position and velocity responses are approximately similar to the RA direction within a bit of change.

VI. CONCLUSION

This study furnishes a practical and low-cost complete control system for real-time remote astronomical observation; it is applicable for small and medium-size telescopes and has been implemented upon the Egyptian 14-inch telescope. This type of observation enables astronomers worldwide to expose sky images remotely for either interaction or robotic operation by executing a series of sequences besides the onsite operation. It will increase international cooperation, simplify astronomy education, reduce the stress of the telescope setting and eliminate traveling efforts. Moreover, despite no physical attendance required, the system is robust enough to protect its equipment and attached devices with self-interruption options in case of risk. The construction of this platform is based on raw packet commands among devices and controllers, which exponentially minimize time consumption in task execution. All electronics, embedded circuits, and sensors are built locally to dispense with commercial automation kits, which are custom-made and expensive. A remote server-client environment has been created via a socket with TCP-IP protocol which provides high performance and adequate security level. The GUI is entirely written in Visual basic under a windows environment regardless any commercial software to be affordable with modification capability. It is not only covering all observing features and aspects but also provides complete monitoring for the whole system precisely. It is affordable and applicable for other observing systems without custom requirements, and this is considered the most significant advantage compared with previous studies regarding robotizing astronomical telescopes. Furthermore, the advanced calculations in coordinates conversion have eliminated the telescope stress in alignment, which require more experience. Finally, it is a complete integrated system where the user does not need to use commercial software to point the telescope, expose sky objects, view fit images, or communicate to the server computer. The cost is significantly affordable compared with commercial kits and other studies. Regarding the telescope performance enhancement, a modified fractional controller ID-T has been employed for the non-linear telescope model to overcome the conventional controller's shortage. An advanced optimization algorithm

POA has tuned this proposed controller to enhance the telescope stability significantly in terms of overshoot, rising, and settling times. This hybrid technique represented in ID-T optimized POA has achieved stability more than twice the best of previous studies, particularly in FLC-PSO. Simulation results refer to the poorness of the TID controller in diminishing the overshoot and prove how the POA produces more accurate results than PSO in our case study.

For future work, it is intended to enhance the telescope pointing efficiency through advanced image processing techniques involving artificial intelligence keeping the observed sky object inside the frame center. It is based on a continuous comparison between the observed and standard images in the catalogs for the same target. The decision toward the best pointing is based on the distribution of the stars surrounding the observed target. In addition, simulation results and output performance of the applied controller are pretty encouraging to be applied experimentally in the future to adapt the remote operation to introduce an intelligent product for observing remotely.

REFERENCES

- [1] M. S. Darwish, A. Shokry, S. M. Saad, M. A. El-Sadek, A. Essam, and M. Ismail, "Kottamia 74-inch telescope discovery of the new eclipsing binary 2MASS J20004638+0547475.: First CCD photometry and light curve analysis," *New Astron.*, vol. 53, pp. 35–38, May 2017.
- [2] A. Bock, E. Axelsson, J. Costa, G. Payne, M. Acinapura, V. Trakinski, C. Emmart, C. Silva, C. Hansen, and A. Ynnerman, "OpenSpace: A system for astrographics," *IEEE Trans. Vis. Comput. Graphics*, vol. 26, no. 1, pp. 633–642, Jan. 2020.
- [3] P. Barmby, "Astronomical observations: A guide for allied researchers," *Open J. Astrophys.*, vol. 2, no. 1, p. 7651, Mar. 2019.
- [4] Y. A. Azzam, A. M. Abd El Hameed, F. S. El-Tokhy, M. Ismail, M. El_harony, and S. M. Sharaf, "Investigation and treatment of the aluminizing process for mirrors of astronomical telescopes and optical instruments of space vehicles," *Appl. Thermal Eng.*, vol. 75, pp. 856–866, Jan. 2015.
- [5] G.-Y. Zhang, J. Wang, P.-Y. Tang, M.-H. Jia, J. Chen, S.-C. Dong, F. Jiang, W.-Q. Wu, J.-J. Liu, and H.-F. Zhang, "An autonomous observation and control system based on EPICS and RTS2 for Antarctic telescopes," *Monthly Notices Roy. Astron. Soc.*, vol. 455, no. 2, pp. 1654–1664, Jan. 2016.
- [6] C. Pennypacker, M. Boer, R. Denny, F. Hessman, J. Aymon, N. Duric, S. Gordon, D. Barnaby, G. Spear, and V. Hoette, "RTML—A standard for use of remote telescopes-enabling ubiquitous use of remote telescopes," *Astron. Astrophys.*, vol. 395, no. 2, pp. 727–731, 2002.
- [7] E. L. Gomez and M. T. Fitzgerald, "Robotic telescopes in education," *Astronomical Rev.*, vol. 13, no. 1, pp. 28–68, Jan. 2017.
- [8] M. Bumbungan, R. Priyatikanto, M. Danarianto, M. Saputra, F. Rohmah, M. Murti, F. Mumtahana, M. Nurzaman, and N. Legita, "Two 0.5-m robotic telescopes for Timau national observatory in eastern Indonesia," *J. Phys., Conf.*, vol. 1231, no. 1, 2019, Art. no. 12008.

- [9] K. Watanabe, M. Otani, H. Tanaka, and M. Okyudo, "The simple and compact remote telescope system," in *Proc. Int. Conf. Complex, Intell. Softw. Intensive Syst.*, Feb. 2010, pp. 1129–1134.
- [10] T. F. Slater, A. C. Burrows, D. A. French, R. A. Sanchez, and C. B. Tatge, "A proposed astronomy learning progression for remote telescope observation," *J. College Teaching Learn.*, vol. 11, no. 4, pp. 197–206, 2014.
- [11] K. M. Riesing, H. Yoon, and K. L. Cahoy, "Rapid telescope pointing calibration: A quaternion-based solution using low-cost hardware," *J. Astronomical Telescopes, Instrum., Syst.*, vol. 4, no. 3, 2018, 034002.
- [12] C. Gutiérrez, D. Arnold, D. Copley, C. Copperwheat, E. Harvey, H. Jermak, J. Knapen, A. McGrath, A. Oria, R. Rebolo, I. A. Steele, and M. Torres, "The new 4-m robotic telescope," *Astronomische Nachrichten*, vol. 340, pp. 40–45, Jan. 2019.
- [13] M. M. Josephine, "Design and construction of a remote control switching device for household appliances application," *Adv. Sci., Technol. Eng. Syst. J.*, vol. 2, no. 4, pp. 154–164, Sep. 2017.
- [14] M. K. Srivastava, A. Ramaprakash, M. P. Burse, P. A. Chordia, K. S. Chillal, V. B. Mestry, H. K. Das, and A. A. Kohok, "TELICS—A telescope instrument control system for small/medium sized astronomical observatories," *Publications Astronomical Soc. Pacific*, vol. 121, no. 884, p. 1112, 2009.
- [15] M. Laas-Bourez, D. Coward, A. Klotz, and M. Boër, "A robotic telescope network for space debris identification and tracking," *Adv. Space Res.*, vol. 47, no. 3, pp. 402–410, Feb. 2011.
- [16] J. Torrejón, J. Berná, and G. Bernabeu, "Real time access to remote telescopes using web based technology," in *Highlights of Spanish Astrophysics III*. Cham, Switzerland: Springer, 2003, p. 510.
- [17] Y. C. Kwon, J. Jeong, Y.-W. Kim, and N. Baek, "An automated astronomical observation system," *Int. J. Control Autom.*, vol. 6, no. 1, pp. 191–200, 2013.
- [18] P. Cuartas-Restrepo, N. Gaviria-Gómez, and J. Galvez-Serna, "Design of a low cost control system for an astronomical observatory," *Ingeniería y Ciencia*, vol. 16, no. 31, pp. 103–127, Jun. 2020.
- [19] L. R. Sonsa, F. Morgado-Dias, and P. Augusto, "Low cost automated astronomical observatory for remote operation: A requisite analysis," in *Proc. Int. Conf. Internet Things Global Community (IoTGC)*, Jul. 2017, pp. 1–6.
- [20] D. Eid, A.-F. Attia, S. Elmasry, and I. Helmy, "A hybrid genetic-fuzzy controller for a 14-inch astronomical telescope tracking," *J. Astronomical Instrum.*, vol. 10, no. 3, Sep. 2021, Art. no. 2150011.
- [21] A.-F. Attia, "Intelligent controller for tracking a 14-inch Celestron telescope," *Acta Polytechnica*, vol. 58, no. 5, pp. 271–278, 2018.
- [22] A.-F. Attia, "Hierarchical fuzzy controllers for an astronomical telescope tracking," *Appl. Soft Comput.*, vol. 9, no. 1, pp. 135–141, Jan. 2009.
- [23] J. Herzog, B. Hofmann, H. Fiedler, M. Prohaska, and T. Schildknecht, "Software and hardware to improve a remote telescope station," in *Proc. 8th Eur. Conf. Space Debris*, 2021, pp. 1–9.
- [24] A. Mansour, F. Elnagahy, and M. Ismail, "An implementation of remotely automated control to the 14-inch telescope system," in *Proc. 15th Int. Conf. Comput. Eng. Syst. (ICCES)*, Dec. 2020, pp. 1–6.
- [25] I. Helmy, A. Hamdy, D. Eid, and A. Shokry, "Autofocusing optimal search algorithm for a telescope system," *J. Astronomical Instrum.*, vol. 10, no. 3, Sep. 2021, Art. no. 2150012.
- [26] M.-H. Jia, Y.-Q. Chen, G.-Y. Zhang, P. Jiang, H. Zhang, and J. Wang, "A web service framework for astronomical remote observation in Antarctica by using satellite link," *Astron. Comput.*, vol. 24, pp. 17–24, Jul. 2018.
- [27] R. Rahim, J. Simarmata, A. Purba, M. A. Prayogi, A. Sapta, O. Krianto, and S. Suharman, "Internet based remote desktop using INDY and socket component," *Int. J. Eng. Technol.*, vol. 7, nos. 2–9, pp. 44–47, 2018.
- [28] A. Tepljakov, E. A. Gonzalez, E. Petlenkov, J. Belikov, C. A. Monje, and I. Petras, "Incorporation of fractional-order dynamics into an existing PI/PID DC motor control loop," *ISA Trans.*, vol. 60, pp. 262–273, Jan. 2016.
- [29] H. R. Patel, S. K. Raval, and V. A. Shah, "A novel design of optimal intelligent fuzzy TID controller employing GA for nonlinear level control problem subject to actuator and system component fault," *Int. J. Intell. Comput. Cybern.*, vol. 14, no. 1, pp. 17–32, Feb. 2021.
- [30] P. N. Topno and S. Chanana, "Differential evolution algorithm based tilt integral derivative control for LFC problem of an interconnected hydro-thermal power system," *J. Vib. Control*, vol. 24, no. 17, pp. 3952–3973, Sep. 2018.
- [31] M. Ahmed, G. Magdy, M. Khamies, and S. Kamel, "Modified TID controller for load frequency control of a two-area interconnected diverse-unit power system," *Int. J. Electr. Power Energy Syst.*, vol. 135, Feb. 2022, Art. no. 107528.
- [32] J. Wang, B. Yang, Y. Chen, K. Zeng, H. Zhang, H. Shu, and Y. Chen, "Novel phasianidae inspired peafowl (*Pavo muticus/cristatus*) optimization algorithm: Design, evaluation, and SOFC models parameter estimation," *Sustain. Energy Technol. Assessments*, vol. 50, Mar. 2022, Art. no. 101825.
- [33] A. Haroon, I. Selim, F. Elnagahy, Y. Azzam, and S. Laban, "Kottamia 14 inch celestron," *J. Astronomical Soc. Egypt*, vol. 14, pp. 59–75, Jun. 2007.
- [34] Celestron. *CGE 1400*. Accessed: 2003. [Online]. Available: https://s3.amazonaws.com/celestron-site-support-files/support_files/CGE1400_11063.pdf
- [35] Starizona. *Focus System*. Accessed: 2022. [Online]. Available: <https://starizona.com/products/microtouch-autofocuser-wired>
- [36] I. Selim, N. Ahmed, and M. Lashin, "Automated of 74-inch kottamia telescope dome based on fuzzy logic due to online weather station data," *Int. J. Comput. Appl.*, vol. 975, p. 8887, Aug. 2016.
- [37] Ash-Dome. *Ash-Dome Description*. Accessed: 2022. [Online]. Available: <http://www.company7.com/mccmo/Ash%20Dome%20catalog.pdf>
- [38] SBIG. *STX-16803 Camera*. Accessed: 2022. [Online]. Available: <https://diffractionlimited.com/product/stx-16803/>
- [39] R. N. Hook, "Polar axis alignment requirements for astronomical photography," *J. Brit. Astronomical Assoc.*, vol. 99, pp. 19–22, Feb. 1989.
- [40] NexStar. *Handset Communication Protocol*. Accessed: 2003. [Online]. Available: https://s3.amazonaws.com/celestron-site-support-files/support_files/1154108406_nexstarcommprot.pdf
- [41] Y. Azzam, K. Kosuge, Z. Wang, A. Alawy, and Y. Hirata, "Telescope automatic alignment and pointing using pattern matching," in *Proc. Int. Conf. Adv. Mechnron., Evol. Fusion IT Mechatronics, ICAM: Abstr.*, vol. 2004, no. 4, 2004, pp. 1–7.
- [42] A. NexStar. *Handset Communication Protocol*. Accessed: 2003. [Online]. Available: http://www.paquetefamily.ca/nexstar/NexStar_AUX_Commands_10.pdf
- [43] J. Meeus. "Astronomical algorithms," *Richmond*, vol. 1, pp. 91–99, 1991.
- [44] T. Taki, "A new concept in computer-aided telescopes," *Sky Telescope*, vol. 77, p. 194, Feb. 1989.
- [45] A. Hamdy, F. Elnagahy, and I. Helmy, "Application of fuzzy logic on astronomical images focus measure," *Turkish J. Electr. Eng. Comput. Sci.*, vol. 27, pp. 3815–3822, Feb. 2019.
- [46] A. B. Smith, D. B. Caton, and R. L. Hawkins, "Implementation and operation of a robotic telescope on skynet," *Publications Astronomical Soc. Pacific*, vol. 128, no. 963, May 2016, Art. no. 055002.
- [47] L. Louis, "Working principle of Arduino and using it as a tool for study and research," *Int. J. Control Autom., Commun. Syst.*, vol. 1, no. 2, pp. 21–29, Apr. 2016.
- [48] T.-B. Huynh, L. Hardy, M. Pezzo, and O. Wilder, "The testing and design of an Arduino microcontroller board for the study of proxemics," *Univ. South Florida St. Petersburg Student Res. J.*, vol. 2, pp. 1–7, Oct. 2012.
- [49] A. B. Smith, D. B. Caton, and R. L. Hawkins, "The development and implementation of a remote robotic telescope system at appalachian state university's dark sky observatory," Ph.D. dissertation, Dept. Eng. Phys., NC Docks, Appalachian State Univ., Boone, NC, USA, 2009.
- [50] Y. Azzam, G. Ali, H. Ismail, A. Haroon, and I. Selim, "Current and future capabilities of the 74-inch telescope of kottamia astronomical observatory in Egypt," in *Proc. 3rd UN/ESA/NASA Workshop Int. Heliophysical Year Basic Space Sci*. Cham, Switzerland: Springer, 2010, pp. 175–187.
- [51] J. Colomé, I. Ribas, X. Francisco, K. Casteels, D. Fernández, J. Isern, X. Palau, and J. Torra, "The OAdM robotic observatory," *Adv. Astron.*, vol. 2010, pp. 1–8, Nov. 2010.
- [52] R. Cedazo, A. Brunete, H. R. Albarracin, and E. Gonzalez, "Open-design for a smart cover of a night-time telescope for day-time use," *Sensors*, vol. 21, no. 4, p. 1138, Feb. 2021.
- [53] M. Gopinathan, S. Sahu, S. Yadava, P. Jangid, B. J. Medhi, P. Rao, B. Kumar, A. Omar, and W. Uddin, "Synchronization of off-centered dome and 3.6 m devasthal optical telescope," in *Software and Cyberinfrastructure for Astronomy IV*, vol. 9913. Bellingham, WA, USA: SPIE, 2016, Art. no. 991340.
- [54] SBIG. *Sbig Ethernet Protocol*. Accessed: 2011. [Online]. Available: https://www.astro.louisville.edu/software/xmccd/archive/xmccd-4.1/xmccd-4.1e/docs/sbig/stx_http_camera_api.pdf

- [55] A. Bihi and J. Granström, "Astronomy software integration with openspace," M.S. thesis, Dept. Sci. Technol., Linköping Univ., Linköping, Sweden, 2020.
- [56] DAVIS-Instruments. *Weather Station*. Accessed: 2022. [Online]. Available: https://cdn.shopify.com/s/files/1/0515/5992/3873/files/07395_234_Manual_VP2_Console_RevZ_web.pdf?v=1656098534
- [57] Vantag-Pro2. *Weather Station Serial Protocol*. Accessed: 2013. [Online]. Available: https://www.nijin.com.tw/file/VantageSerialProtocolDocs_v261.pdf
- [58] L. K. Hardy, T. Butterley, V. S. Dhillon, S. P. Littlefair, and R. W. Wilson, "Pr5m—A 0.5 m robotic telescope on La Palma," *Monthly Notices Roy. Astronomical Soc.*, vol. 454, no. 4, pp. 4316–4325, Dec. 2015.
- [59] J. Slotine and L. Weiping, *Applied Nonlinear Control*, vol. 199, no. 1. Englewood Cliffs, NJ, USA: Prentice-Hall, 1991.
- [60] M. A. El-Dabah, S. Kamel, M. Khamies, H. Shahinzadeh, and G. B. Gharehpetian, "Artificial gorilla troops optimizer for optimum tuning of TID based power system stabilizer," in *Proc. 9th Iranian Joint Congr. Fuzzy Intell. Syst. (CFIS)*, Mar. 2022, pp. 1–5.
- [61] M. A. El-Dabah, S. Kamel, M. A. Y. Abido, and B. Khan, "Optimal tuning of fractional-order proportional, integral, derivative and tilt-integral-derivative based power system stabilizers using Runge Kutta optimizer," *Eng. Rep.*, vol. 4, no. 6, Jun. 2022, Art. no. e12492.
- [62] S. Kumari and G. Shankar, "Novel application of integral-tilt-derivative controller for performance evaluation of load frequency control of interconnected power system," *IET Gener., Transmiss. Distrib.*, vol. 12, no. 14, pp. 3550–3560, Aug. 2018.
- [63] E. A. Mohamed, E. M. Ahmed, A. Elmelegi, M. Aly, O. Elbaksawi, and A.-A. A. Mohamed, "An optimized hybrid fractional order controller for frequency regulation in multi-area power systems," *IEEE Access*, vol. 8, pp. 213899–213915, 2020.
- [64] T. Krzeszowski, K. Wiktorowicz, and K. Przednowek, "Comparison of selected fuzzy PSO algorithms," in *Recent Advances in Computational Optimization: Results of the Workshop on Computational Optimization WCO 2016*, vol. 717. Cham, Switzerland: Springer, 2017, pp. 107–122.
- [65] S. Mirjalili and A. Lewis, "The whale optimization algorithm," *Adv. Eng. Softw.*, vol. 95, pp. 51–67, Feb. 2016.
- [66] K. Singh, M. Amir, F. Ahmad, and M. A. Khan, "An integral tilt derivative control strategy for frequency control in multimicrogrid system," *IEEE Syst. J.*, vol. 15, no. 1, pp. 1477–1488, Mar. 2020.
- [67] Z. Li, "The optimization design of PID controller parameters based on particle swarm optimization," in *Proc. 5th Int. Conf. Adv. Mater. Comput. Sci.*, Qingdao, China, 2016, pp. 460–484.
- [68] B. J. Lurie, "Three-parameter tunable tilt-integral-derivative (TID) controller," U.S. Patent 5 371 670, Dec. 6, 1994.
- [69] K. K. Deveerasetty, Y. Zhou, and B. Han, "Trajectory tracking of a quadrotor using TID controller," in *Proc. Austral. New Zealand Control Conf. (ANZCC)*, Nov. 2019, pp. 139–144.



S. H. ELBANNA was born in Kafer El-Sheikh, Egypt, in July 1960. He received the B.Sc. (Hons.) and M.Sc. degrees in electrical engineering (power and machines sector) from Al-Azhar University, Egypt, in 1985 and August 1990, respectively, and the Ph.D. degree in electrical engineering (power and machine sector) from Al-Azhar University, in August 1997, according to the channel system between Berlin and Al-Azhar University. Since 2003, he has been an Associate Professor at Al-Azhar University. Since 2008, he has been a Professor at Al-Azhar University. He has been a Professor at Umm Al-Qura University, Saudi Arabia, from 2008 to 2017. He has supervised and discussed more than 22 M.Sc. and 13 Ph.D. thesis. Also, he has excellent scientific cooperation with famous research institutes in Germany and Egypt through different funded research projects and thesis supervision. He has designed and supervised several projects with the General Organization for Physical Planning, Cairo, Egypt. He has published more than 39 technical papers in various international journals and conferences. His current research interest includes control of power systems using artificial intelligence.



MAHMOUD A. EL-DABAH was born in Kafr El-Shaikh, in 1985. He received the B.Sc., M.Sc., and Ph.D. degrees from the Faculty of Engineering, Al-Azhar University, Cairo, Egypt, in 2007, 2012, and 2016, respectively. He is currently an Associate Professor with the Electrical Engineering Department, Faculty of Engineering, Al-Azhar University. His research interests include power systems operation, control, planning, optimization, and renewable energy resources integration in electrical power systems. He is a Reviewer of several journals, such as IEEE Access, *Energies*, and IET, and different springer nature journals.



FARAG ELNAGAHY was born in Cairo, in 1967. He received the B.Sc. degree in electronic engineering from the Faculty of Electronic Engineering, Menoufia University, Egypt, in 1990, the M.Sc. degree in systems & computers engineering from the Faculty of Engineering, Al-Azhar University, Cairo, Egypt, in 1998, and the Ph.D. degree in electrical engineering and informatics from the Faculty of Electrical Engineering, Czech Technical University in Prague, in 2004. He is currently an Associate Professor with the Astronomy Department, National Research Institute of Astronomy and Geophysics (NRIAG), Cairo. His research interests include image processing, coding, pattern matching, and neural networks.



MOHAMED ISMAIL was born in Qalyubiya, Egypt, in 1983. He received the B.Sc. degree in electrical engineering, power and electric machines sector from Banha University, Egypt, in 2005, and the M.Sc. degree in electrical engineering in automatic control from Helwan University, in 2012. He is currently pursuing the Ph.D. degree in electrical engineering with the Faculty of Engineering, Al-Azhar University, Egypt. He is also a Research Assistant with the Astronomy Department, National Research Institute of Astronomy and Geophysics (NRIAG), Cairo, Egypt. His research interests include automatic control, electric systems analysis and modeling, and optimization-based artificial intelligence for solving non linear problems. Furthermore, experimentally, he has an experience in astronomical automation and instrumentation.